NTNU
Norwegian University of
Science and Technology

Optimization of the casting process for silicon nitride crucibles
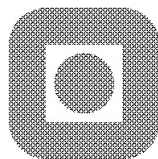
Ermis Kanakakis

Optimization of the casting process for silicon nitride crucibles

Ermis Kanakakis

Supervisor: Professor Eiving Johannes Øvrelid

Co-Supervisors: Professor Marisa Di Sabatino Lundberg

Dr. Arjan Ciftja

Department of Materials

Norwegian University of Science and Technology

Acknowledgements

First and foremost, I would like to express my deep gratitude to my supervisor, Eivind Johannes Øvrelid, for his valuable guidance and advice as well as my co-supervisors Marisa Di Sabatino and Arjan Ciftja who contributed to the realization of this project. Their guidance helped me throughout a whole year of research and writing for this thesis. I would also like to thank all the experts who got involved in my project. Their help was crucial and each one added their small bit which, in the end, was a sine qua non. Finally, words will never be enough to thank my family for their constant support, both financial but mostly emotional, despite the numerous obstacles I faced during this year.

Ermis Kanakakis

Abstract

As renewable energy sources get to replace conventional fossil fuel power plants, solar cells will come to play a major role. For this purpose, their efficiency must be enhanced and their cost minimized in order to compete with alternative forms of power such as hydroelectric or wind. A major part of the cost during solar cell fabrication belongs to the expense for the crucible required for crystal growth. So far, on industrial scale, crucibles are non-reusable, which means that they need to be replaced after each use. The aim of this work was to:

1. Test the influence of oxidation on the wetting properties of Si_3N_4

2. Define alternative types of coatings for directional solidification casting of Si

3. Develop a new process for casting in small crucibles

Surface oxidization of Si_3N_4 reduces its wettability and acts as a barrier that prevents impurity diffusion into the silicon melt during solidification. Small Si_3N_4 samples were heat-treated under various temperatures and durations. Surface oxidation and the formation of a silicon oxynitride layer were tested. Afterwards, four cylindrical and four conical Si_3N_4 crucibles were heat-treated at 1200^oC in order to get their surfaces oxidized. All of the cylindrical crucibles were destroyed by cracks and excessive flaking during heat-treatment or coating. Three of the conical ones were further treated using different coatings and one was left uncoated. The coatings were: a) Normal Si_3N_4 powder; b) Colloidal silica mixed with Si_3N_4; c) BaO intermediate layer and normal Si_3N_4 on top. P-type silicon ingots were grown in all of them. Subsequently, the ingots were removed and cut in order to be characterized. The ingot grown in the uncoated crucible was strongly attached to the substrate and was impossible to remove. Finally, samples from the rest three ingots were acquired and characterized by measuring their resistivity, minority carrier lifetime and impurity concentration (interstitial oxygen and substitutional carbon).

The ingot grown in the crucible with normal Si_3N_4 powder coating showed the highest average lifetime. The ingot from the colloidal silica mix was very clean which means that the mechanical stability of the coating had increased. It also had the lowest oxygen concentration, a fact which suggests that coating dissolution into the melt had been limited. However, metallic impurities from the crucible had killed lifetime completely. Finally, the ingot from the BaO

coated crucible showed no particular improvement in comparison to the normal one and its fluctuating resistivity suggests that a lot of oxides had formed during solidification.

Contents

Acronyms and symbols

BSE Backscattered Electrons

DS Directional Solidification

EDS Energy Dispersive Spectroscopy

FPP Four Point Probe

FTIR Fourier Transform Infrared Spectroscopy

mono-Si Monocrystalline Silicon

multi-Si Multicrystalline Silicon

QSSPC Quasi Steady State Photoconductance

SEM Scanning Electron Microscope

SE Secondary Electrons

VGF Vertical Gradient Freeze

μW-PCD Microwave Photoconductance Decay

c_L Concentration of impurity in liquid

c_S Concentration of impurity in solid

c(x) Oxygen concentration

C$_s$ Substitutional Carbon

f_s Fraction of solidified ingot

G Electron-hole pair generation rate

k distribution coefficient

N_d donor concentration

O$_i$ Interstitial Oxygen

r Average pore channeel radius

s Distance between two probes in FPP technique

γ_{LV} Liquid surface tension

γ_{SV} Solid free surface energy

γ_{SL} Interfacial liquid-solid tension

δ Secondary electron coefficient

Δ**n** Excess carrier density

η backscattered electron coefficient

θ Contact angle

μ_n electron mobility

ρ resistivity

σ conductivity

τ_{eff} Effective minority carrier lifetime

τ_{bulk} Bulk lifetime

τ_{surf} Surface lifetime

τ_{rad} Radiative recombination lifetime

τ_{Aug} Auger lifetime

τ_{SRH} Shockley-Read-Hall lifetime

Chapter 1

Introduction

With the current demands for electricity and due to the rapid climate change we are facing in the 21st century, it is essential that renewable energy technologies be constantly improved in order to compete with fossil fuels. The earth is constantly exposed to sunlight of power density around 1kW per square meter. Harvesting just a portion of this energy would be a priceless contribution to meeting the global electricity needs.

The dominant material in today's solar cell industry is still silicon, mainly due to its abundance, efficiency and stability. Furthermore, the share of multi-crystalline Si in 2015 was 68% of the total with 43.9 GWp annual power production [1]. Hence, optimizing solar cell performance and fabrication is currently one of the most researched scientific fields. Another factor that will determine the future of photovoltaics is their price per kWp compared to other renewable sources of energy.

According to the International Technology Roadmap for Photovoltaic [2], 16% of mc-Si module cost is due to the wafer construction. A significant portion of this amount is spent on the crucible in which the raw material (feedstock) is melted. On industrial scale, the most common crucibles are made of fused silica and they can only be used once. Thus, developing methods that will allow the reusability of crucibles will greatly reduce the total cost of silicon solar cells.

In addition, a possible candidate should satisfy some crucial parameters such as low contamination of the silicon ingot and non-sticking (wetting) behaviour during the ingot growth. Impurities play a key role in solar cell performance. Contamination due to the feedstock itself, the crucible and the environment reduce minority carrier lifetime. Especially near the edges of

the ingot, the impurities caused by diffusion from the crucible cause the, so called, red zone, a region in the crystal that exhibits extremely low performance and needs to be removed. Therefore, contamination needs to be kept as low as possible.

One material that could replace fused silica crucibles, due to its mechanical and chemical stability, is Silicon Nitride (Si_3N_4). The most important aspect of silicon nitride being used as crucible material is its reusability. Quartz crucibles are used only once due to their phase-transformation in high temperature, which results in cracks during cooling of the ingot. Silicon nitride does not undergo a phase transformation and withstains its mechanical and thermal properties over the temperature range. Therefore, it can be used several times. In addition, since it is oxygen free, provided that everything else is the same (impurity content, crystallization technique, coating etc.), it should enhance the efficiency of the solar cells compared to oxide crucibles.

However, in order to be used several times, the silicon ingot must be effectively removed from the crucible without damaging it. For this to happen, the silicon melt should not wet and stick to the crucible walls. Si_3N_4 is wetted by molten silicon whereas SiO_xN_y is not (silicon oxynitride). Therefore, oxidation of nitride crucibles by heating it to high temperatures, or by applying oxide or oxide-containing coatings is important.

In this work, we aimed to investigate the effect of alternative coatings and oxidation of silicon nitride crucibles. Small Si_3N_4 crucibles were provided by Steuler Solar Advanced Ceramics. Heat-treatment in various conditions was tested to achieve the optimal oxidation level. Two alternative coating methods were studied in comparison against the industrial standard. Finally, directional solidification silicon casting was tested. For the purpose of the whole project, new methods of coating, casting and characterization needed to be developed.

It is important to take into consideration that all our experiments were done in small laboratory scale and, therefore, it is expected that quality characteristics will improve on industrial applications. A factor that highly affects silicon purity is the surface-to-volume ratio of the material that is in contact with the crucible substrate or the atmosphere on top of the melted Si. This ratio needs to be as low as possible in order for the red zone to be proportionally minimal.

Chapter 2

Theory and Background

2.1 Properties of materials

2.1.1 Multicrystalline Silicon and Feedstock

Silicon is one of the most abundant chemical elements on earth. It is a member of the 14th group of the periodic table (along with carbon, germanium et al). It has 4 electrons in its outermost shell and forms diamond crystal lattice (see Figure 2.1). It has a melting point of 1687K (1414°C) when in pure form. Silicon is classified according to its level of purity. For solar cell applications, silicon must be at least 99.9999% pure, commonly referred to as 6N (six nines) pure.
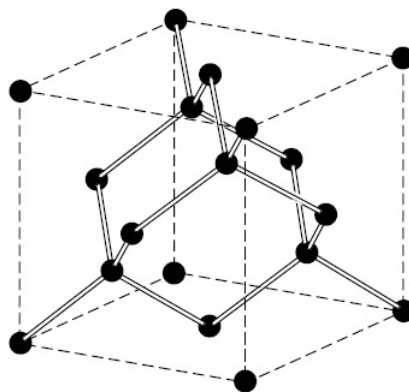
Figure 2.1: Crystal structure of diamond showing the tetrahedral bond arrangement. [3]

The three most common types of silicon are mono-crystalline, multi-crystalline and amorphous. Each of them consists of smaller parts of perfectly oriented crystal structures, called

grains. The main distinction between each type is grain size. In the case of multi-Si, which was the type investigated, grain size is 1mm-10cm [4].
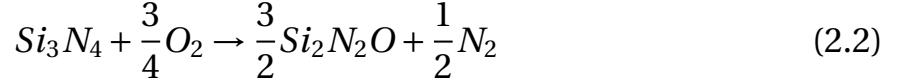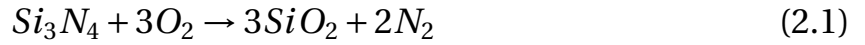

Figure 2.2: a) Multi-Si across the grain boundaries. b)A 10x10cm textured multi-Si wafer. Grains of different orientation appear with different colour. [5]

Another important physical property of silicon is its density, which is higher in liquid (2420 kg/m^3) than in solid phase (2300 kg/m^3) [6]. Therefore, it is expected to expand as it solidifies and can cause cracks or complete destruction of the crucible. One way of dealing with this problem is by using the method of directional solidification.

2.1.2   Silicon Nitride and Oxidation Mechanisms

Silicon Nitride is a light-gray material with a very high melting point (1900$^o C$). It is chemically inert and thermodynamically stable at high temperatures. However, its wetting behaviour when in contact with liquid silicon makes it an inappropriate material for crucibles.

A study by Ogbuji and Jayne [7] suggests that heat treatment of Si_3N_4 at 1100$^o C$ in the presence of oxygen causes thermal oxidation through progressive substitution of N by O. Thermodynamically, the oxidation process was described by Honghua et al. [8] in the two following chemical equations:

$$Si_3N_4 + 3O_2 \rightarrow 3SiO_2 + 2N_2 \tag{2.1}$$

$$Si_3N_4 + \frac{3}{4}O_2 \rightarrow \frac{3}{2}Si_2N_2O + \frac{1}{2}N_2 \tag{2.2}$$

Moreover, Portz and Thummler examined the oxidation of reaction-bonded silicon nitride (RBSN) in proportion to the material's porosity [9]. Both studies showed that the ratio of N:O on a cross section of the silicon oxynitride ($SiN_{2-x}O_{2+x}$) varies along different depths. Furthermore, a SiO_2 crust is formed on top of the oxynitride layer.
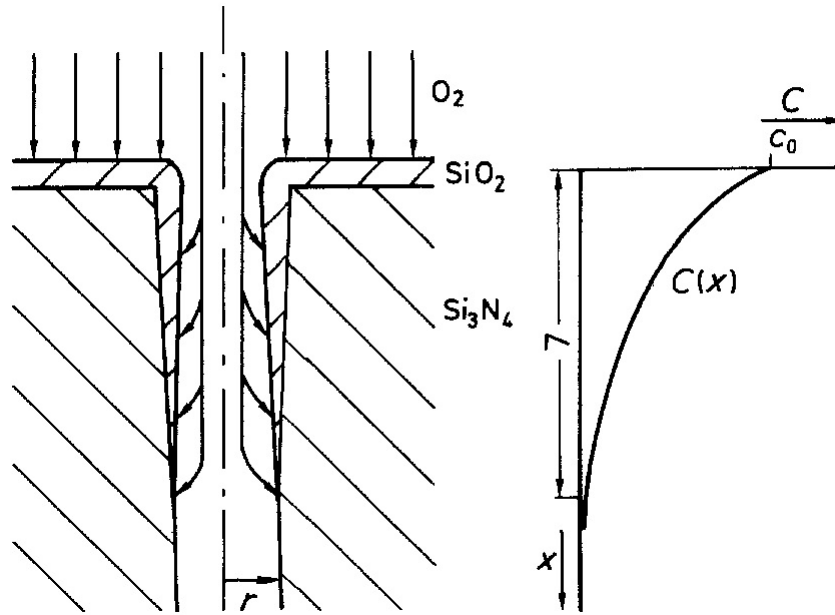
Figure 2.3: Diffusion on oxygen through a pore channel on Si_3N_4 [9]

In more detail, oxidation of silicon nitride takes place in two stages. First, under the right temperature and pressure, oxygen diffuses through the pores and reacts with Si_3N_4 forming SiO_2 as can be visualized in figure 2.3. In order to describe the process we assume an average channel radius, r. As oxygen flows inside the pore, its concentration is reduced due to oxidation of the channel surfaces. We can define the oxygen concentration as c(x), where x is the distance from

the specimen surface and the concentration at the surface to be constant and equal to c_0. For a constant channel radius, r, the depth, L, of the oxidation depends on the reaction time, t_R and the transport time, t_D.

When the pore channels have been sealed by oxygen, no more diffusion is allowed into the specimen, and the second stage begins. The only space where further oxidation is permitted is the outer surface of the sample. It is expected that the total internal oxidation strongly depends on heat treatment conditions and structure of the specimen.

Different studies [10], [11] have also shown that the presence of oxygen on the surface of silicon nitride creates a protective layer that prohibits wetting. Therefore, the (Si_3N_4) crucibles that were tested during the project underwent heat treatment that caused the sintering of oxygen on their surface and the formation of a protective silicon oxynitride layer.
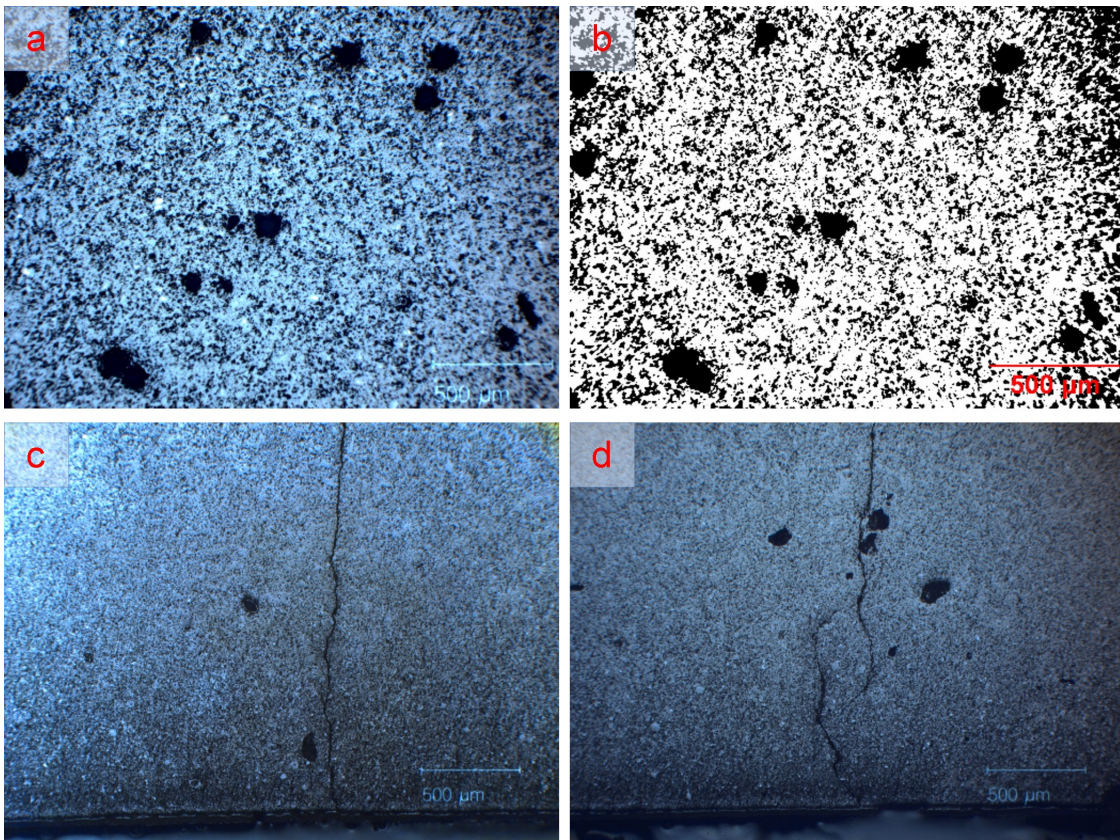

Figure 2.4: Electron microscopy images of a Si_3N_4 surface: a) area in the sample with high porosity; b) B&W duplicate; c,d) cracks near large pores

Electron microscopy images showing the Si_3N_4 surface were acquired by my co-supervisor Dr. Arjan Ciftja (see fig.2.4). In these pictures, the porosity of the material is clearly visible and,

after creating a B&W duplicate, the pores were calculated to occupy roughly 29% of the sample's surface and their average radius was found 6.5μm, by using a circular pore approximation. In addition, cracks seemed to occur near the largest pores, a fact which could potentially be problematic in case oxidation and thermal expansion created mechanical stress.

2.1.3 Wettability of ceramics

A critical parameter for crystal growth is the wetting behaviour of the crucible. When a drop of liquid comes in contact with a solid substrate, electrostatic forces between them will define the shape of the liquid. If the surface energy is high enough, the droplet will spread and, in extreme cases, cover the entire substrate surface.
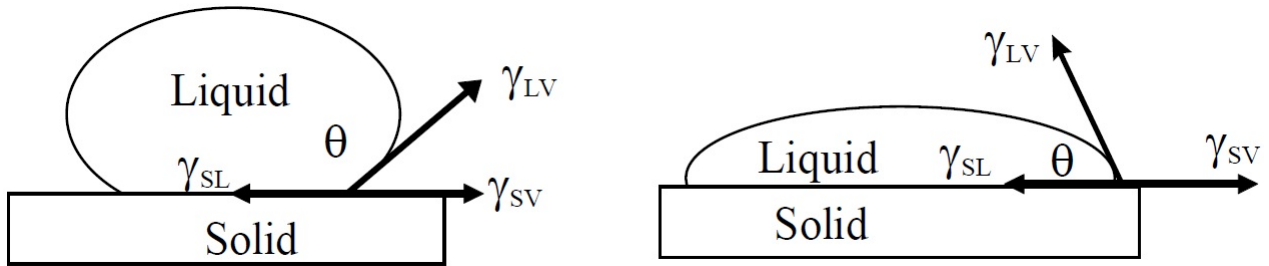

Figure 2.5: The contact angle between the liquid droplet and the substrate defines the wetting properties of the liquid-solid interface. [12]

Wettability is quantitatively defined by the contact angle, θ (see figure 2.5). There is a relationship between θ, the liquid surface tension, γ_{LV}, the solid free surface energy, γ_{SV} and the interfacial tension between liquid and solid, γ_{SL}. This relationship is described by Young's equation:

$$\gamma_{SV} = \gamma_{SL} + \gamma_{LV} \cdot cos\theta \qquad (2.3)$$

If the liquid droplet is nonwetting ($\theta > 90^o$), it will form a bead, achieving minimum contact with the solid. On the contrary, for contact angles lower than 90°, the liquid is defined as wetting.

It is essential that molten silicon is nonwetting when in contact with the crucible. If not, it will stick during solidification and the extraction of the ingot will require the crucible's de-

struction. Therefore, a coating is usually applied on the crucible, as described below, in order to minimize wettability properties of Si.

2.1.4 Coating Properties

In the process of Si ingot growth, the standard approach requires coating of the interior surface of the crucibles. This coating acts as an intermediate layer between the crucible and the melt, and its purpose is to prevent adhesion. Another crucial parameter of the coating is to minimize contamination in the final product. Furthermore, part of the coating will always dissolve into the silicon melt. In case this phenomenon is too intense, the silicon can stick to the crucible, making its detachment infeasible without breaking part of it. As a result, the coating material must be carefully selected and applied. For our experiments, three different coatings were tested and compared.

Si_3N_4 based coating

A common characteristic of all nitrides is their high chemical and thermal stability. According to information provided by H.C. Starck Ceramics GmbH [13], Si_3N_4-based coating not only allows removal of the Si ingot after solidification but also acts as a barrier preventing the diffusion of impurities into the melt and the reaction between the silicon and the crucible. Furthermore, its wear resistance and low degree of thermal expansion make it the most common ceramic used for crucible coating.

Colloidal Silica

Although Si_3N_4 is chemically and thermally stable, its mechanical resistance is often limited. As a result, a pure Si_3N_4 coating has been reported by Rancoule [14] to flake off during or even before use. Hence, methods have been suggested in order to enhance the mechanical resistance of the coating by introducing materials with high binding abilities in the mix. A 5% mix of Colloidal Silica (aqueous solution of nano-scale silica particles) in Si_3N_4 powder was investigated by Rancoule and the results showed improved mechanical resistance while the full effectiveness of the silicon nitride grains was maintained.

Barium Oxide

A way of further increasing the quality and purity of the final product is by minimizing contamination from the crucible. One material that has been widely used in the silica crucible coating process as devitrification promoter is Barium oxide (BaO). For this purpose, a Barium Hydroxide anhydrous (Ba(OH)$_2$) powder, by Alfa Aesar, with 94%-98% purity was used. It was dissolved in warm, distilled water and a saturated solution was used to soak one of the crucibles. Afterwards, the crucible was left overnight in a hot chamber (150°C) to dry and, finally a normal Si$_3$N$_4$ coating was applied on top (heating up to 1200°C). According to Hsieh et al. [15], during this process, carbon dioxide from the atmosphere reacts with the (Ba(OH)$_2$), forming barium carbonate which subsequently reacts again, resulting in the formation of an intermediate BaO layer between the crucible and the Si$_3$N$_4$ coating.

2.2 Impurities

Impurities are introduced in the crystal lattice during both the solidification and the cooling process and can either be inserted on purpose (such as in doping) or accidentally from the environment. Apart from the dopants, the most common elements found in the silicon ingot are oxygen, nitrogen, carbon and iron. Smaller traces of other metals such as aluminium and copper can be found, depending on the purity of the crucible and feedstock. Impurities influence the solar cells' efficiency because they introduce energy levels in the band gap and act as traps. The closer those levels lie to the middle of the band gap the easier it is for electrons in the conduction band to use them as intermediate energy levels and recombine with holes in the valence band. In addition, defects such as grain boundaries and dislocations can act as recombination centres. With increasing impurity concentration, also rises their electrical activity. Therefore, impurities are an important parameter in the solar cell's overall performance and we will devote this section in summarizing their main characteristics and how they get incorporated in the silicon.

Oxygen

Oxygen is one of the most common impurities and is mainly introduced by the feedstock and the crucible. Part of the dissolved oxygen can, then, evaporate from the top surface. There are two ways that it can be incorporated in the final ingot. It can either appear as interstitial atoms $[O_i]$ spread out in the crystal or as precipitates. According to a study by Häßler et al. [16] the first case does not affect the material's performance. On the other hand, oxygen precipitates affect both the electrical and mechanical properties of the crystal. Even though O_i does not directly contribute to carrier recombination, it promotes the formation of precipitates and therefore, needs to be minimized. In our case, both the crucibles and the coatings were highly oxidized and it is expected that oxygen levels are significant in the final product, especially due to the small ingot size. High oxygen levels in the ingot are also indicating excessive dissolution of the coating into the melt during solidification.

Carbon and Nitrogen

Carbon is an element with the same number of electrons as silicon in its outermost shell (isovalent impurity) and can, therefore, be incorporated in the crystal lattice as a substitutional element $[C_s]$. When oxygen atoms get in contact with the graphite insulation in the furnace, carbon monoxide forms, which can dissolve into the molten silicon through the top surface. It can also be originally present in the crucible and dissolve into the silicon through the coating. Nitrogen is another common impurity in solar silicon. Usually, it originates from the Si_3N_4 coating but, in our case, it is expected to have a higher concentration in the ingot due to the nature of the crucibles.

Even though they are both electrically inactive, they can promote the formation of oxygen precipitates and cause the formation of SiC and Si_3N_4 particles which will accumulate lifetime-killing impurities, but can also form dislocations [17][18]. On the other hand, studies have shown that both carbon and nitrogen can improve the electrical properties of silicon crystals by neutralizing the defects [19][20].

Iron

Iron is the most common metallic impurity in multicrystalline silicon. This fact, in combination with its electrical and kinetic properties, makes iron the impurity with the highest impact for lifetime deterioration. Interstitial iron introduces deep levels in the band gap, thus creating recombination centres. Although iron has a low distribution coefficient in silicon and, during solidification, most iron segregates to the top of the ingot, it can, afterwards, diffuse back to the solid bulk. In addition, iron precipitated at defects such as grain boundaries, dislocations or oxygen is much more mechanically stable, but can still act as an impurity source at hight temperature (for example, during emitter diffusion and contact firing)[21]. Iron can originate both from the feedstock and the crucible/coating but also from the furnace environment. Figure 2.6 summarizes the most important impurities and their source.
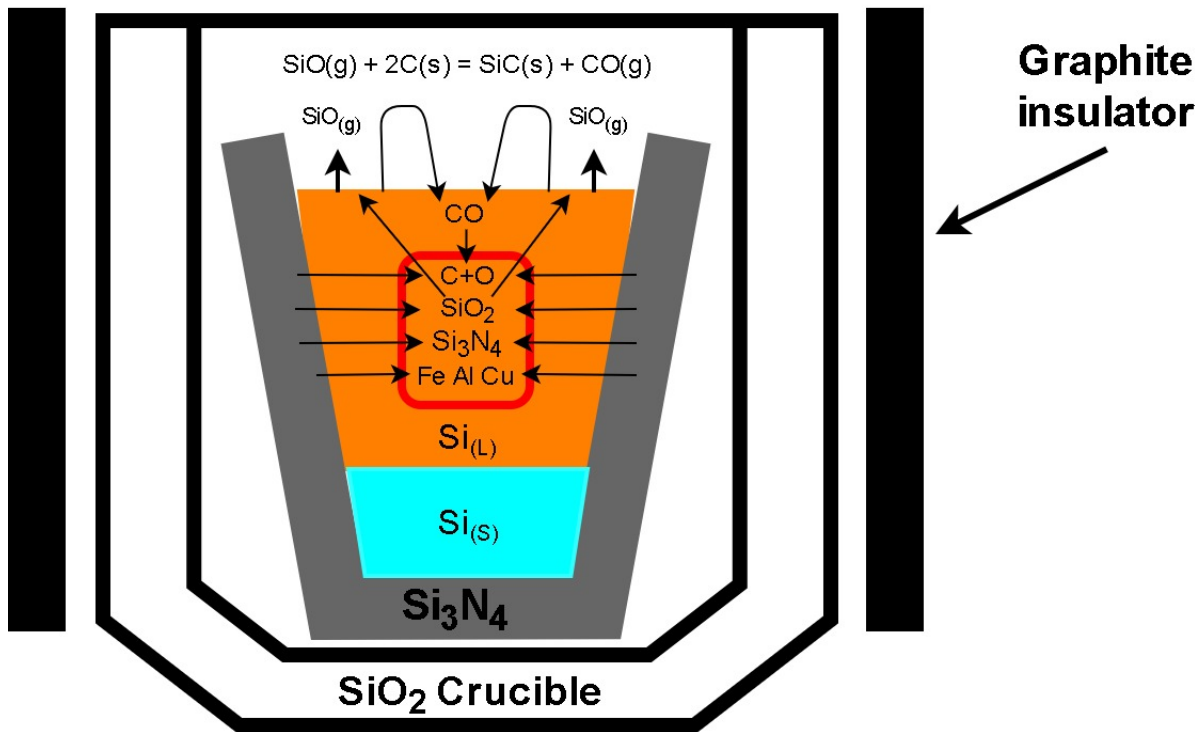

Figure 2.6: The most common impurities found in a silicon ingot (enclosed in the red rectangle) and their source

2.2.1 Axial segregation

Along the crystal ingot, impurities are usually found in different amounts. This is caused because their solubility differs from liquid to solid state. The ratio of solid-to-liquid across the interface is given by the distribution coefficient:

$$k = \frac{C_S}{C_L} \tag{2.4}$$

where C_S and C_L are the solid and liquid concentrations, respectively.

Usually, k<1, which means that impurities have higher solubility in liquid than in solid form. As a result, impurities tend to segregate towards the top of the ingot. When describing solute variations in the crystal growth process it is normally assumed that we have complete mixing (homogeneity) of solutes in the liquid and no diffusion can happen in the solid part. The concentration of solute in the solidified part is, then, given by Sheil's equation:

$$C_S = k \cdot C_0 (1 - f_S)^{(k-1)} \tag{2.5}$$

where C_0 is the initial concentration of solute in liquid form. The concentration of solid solute at the beginning (when $f_s = 0$) is, according to Equation 2.5, $k \cdot C_0$ and decreases as we move further up which means that the liquid gets richer and richer in solute during the process. Consequently, the doping concentrations increase along the ingot. A schematic representation of this distribution is shown in Figure 2.7
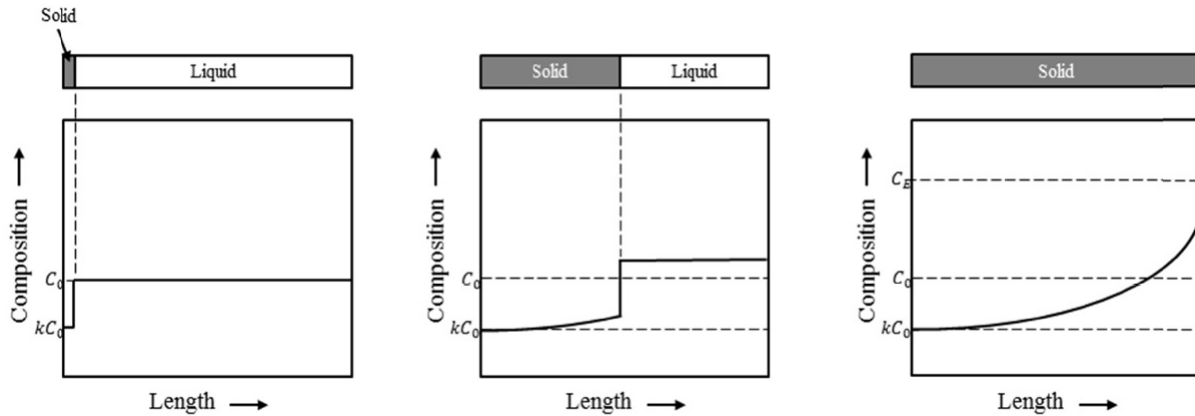
Figure 2.7: Schematic representation of the solute distribution during crystal growth process. Three stages are depicted: (left) beginning of solidification, (middle) 50% of the process and (right) after complete solidification. Picture taken from NTNU PhD thesis of Guilherme Gaspar [22]

2.3 Experimental Methods

2.3.1 Scanning Electron Microscope (SEM)

Scanning electron microscopy is one of the most powerful tools in research. In contrast with conventional microscope, SEM allows the observation and characterization of the most kinds of materials on a scale down to a few nanometres. It also has the capability of acquiring information from deeper layers of the sample, thus creating a three-dimensional profile of the material. In the SEM, an electron beam is firstly accelerated by a high voltage. Subsequently, a magnetic field created by an electromagnet (magnetic lens) exerts Lorentz force on the beam causing it to shrink in diameter. Alterations in electromagnet current flow have a direct impact on the focal point of the lens. A simplified schematic overview of the SEM apparatus is depicted in figure 2.8.

The focused electron beam reaches the sample and is swept across its surface. Various kinds of interactions give rise to backscattered electrons (BSE), secondary electrons (SE), Auger electrons, characteristic and continuous X-Rays and heat as shown in figure 2.9. These signals strongly depend upon the energy of the primary beam and the atomic number of the specimen. For the purpose of this master thesis, BSE, SE and X-Rays signals were examined and those methods will be further discussed below.
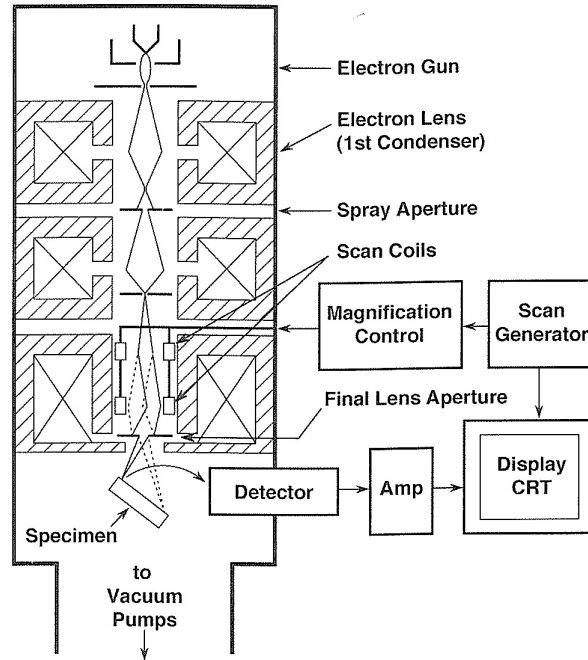
Figure 2.8: Schematic representation of the SEM column. The electron gun, lenses and detector are depicted. [23]

Backscattered Electrons (BSE)

Backscattered electrons are electrons initially coming from the beam. After they reach the sample, they undergo one or several elastic collisions with the specimen nuclei (see figure 2.11). A proportion of them manages to exit the specimen as backscattered electrons. The ratio of backscattered electrons, n_{BSE}, to the initial number of electrons in the beam, n_B, is defined by the backscattered electron coefficient, η.

$$\eta = \frac{n_{BSE}}{n_B} \tag{2.6}$$

The backscattered electron coefficient is strongly dependent on average atomic number, Z. For low atomic numbers, scattering mechanisms are weak and only a small number of the initial beam electrons is returned as BSE. As the atomic number increases, the BSE signal rises too. As a result, information regarding the elemental constitution of the specimen can be visualised.
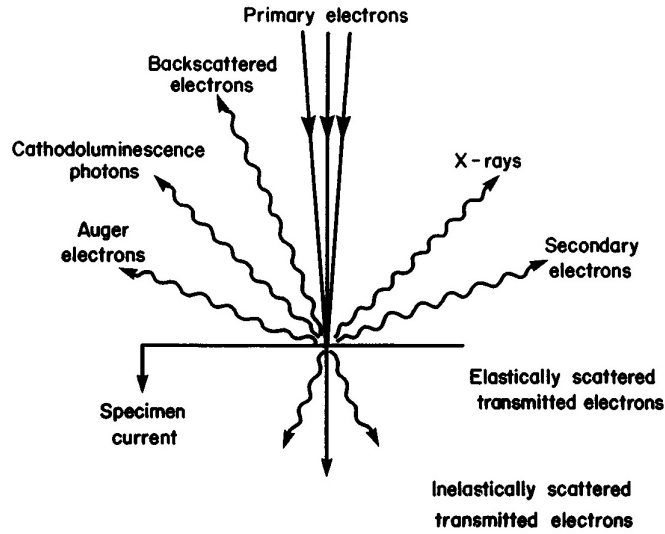
Figure 2.9: Different signals emerging from the interaction between the primary electron beam and the specimen. [24]

Secondary Electrons (SE)

Secondary electrons are emitted from the specimen atoms when beam electrons collide with loosely bound electrons of outer shells (see figure 2.11), thus gaining enough kinetic energy to escape their orbitals. They are characterized by extremely low energies (typically <50eV) which makes them unlikely to escape from the sample if they originate at a depth bigger than 50Å. As a result, these electrons provide information about surface morphology of the specimen. The total SE coefficient, δ, is given by

$$\delta = \frac{n_{SE}}{n_B} \tag{2.7}$$

where n_{SE} is the number of secondary electrons generated by a beam of n_B number of primary electrons.

Since SE are former bound electrons of outer orbitals in the specimen, they are not dependent on atomic mass. Due to the complexity of scattering processes, it has been a challenging task to accurately predict the coefficients η and δ. In 1966, after long experimental investigations, Heinrich and Wittry came up with the empirical dependence of BSE and SE on the atomic
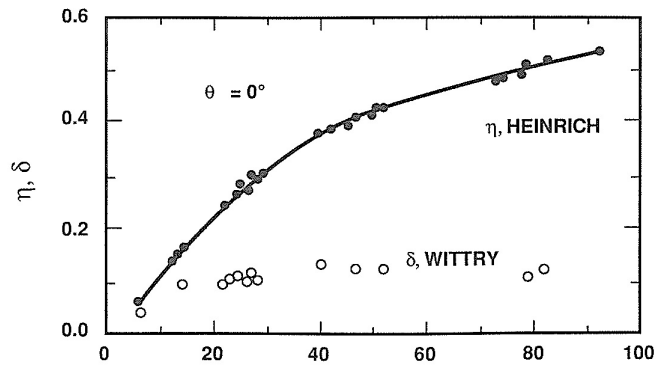
number as seen in figure 2.10.

Figure 2.10: Backscattered electron and secondary electron coefficients as a function of atomic number [23]

Energy Dispersive Spectroscopy (EDS)

When a beam electron reaches an atom of the specimen, it can interact with an inner orbital electron and eject it from its shell. This leaves an empty space in this orbital and the atom becomes an unstable excited ion as shown in figure 2.11. A specific set of allowed transitions will cause the atom to relax to its ground state. For each element, atomic energy levels are sharply defined. Consequently, the energy difference between different orbitals is also characteristic. In the case of X-Ray emission, this energy difference is emitted as electromagnetic radiation of well-defined energy.

2.3.2 Operating Principle of Thermocouple

A thermocouple is a device used to give real time measurements of high temperatures. It consists of two dissimilar wires, called thermoelements, fusion-welded at one end (see figure 2.12). Their other end is kept at a constant temperature, T_R and connected to our system through a reference junction. By applying heat at the measuring junction, the temperature rises to T_M and a voltage is produced between the two thermoelements. This voltage is called electromotive force (EMF) and depends on the temperature difference between the two junctions and the material of the thermoelements. Thermocouples are usually enclosed in ceramic tubes to prevent them from creating short circuits along the way and, also, to protect them from the environment.
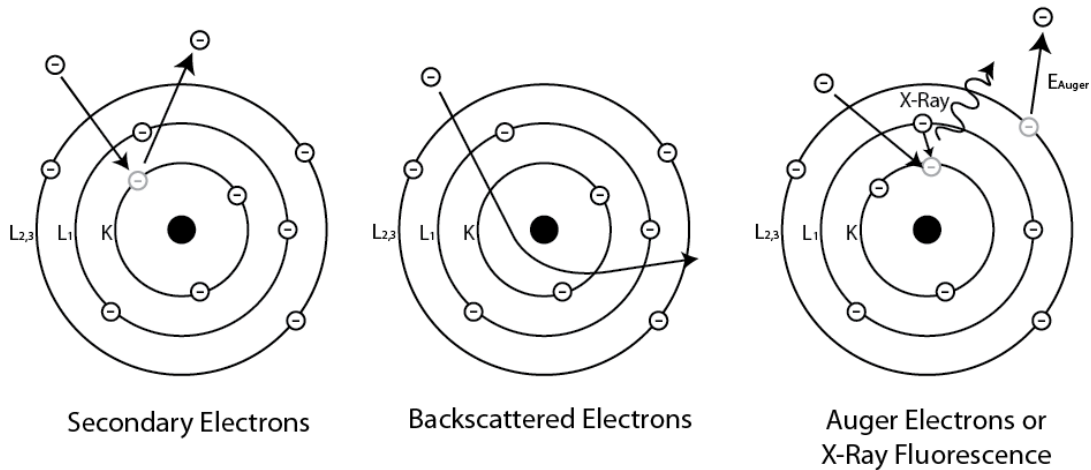
Figure 2.11: Different kinds of emissions upon impact of the incident electron. Secondary electrons emerge after inelastic collisions and backscattered electrons are elastically scattered. Larger nuclei can deflect more of the incoming electrons, increasing the signal strength. Finally, Auger and X-Rays are caused by an ejected electron in a lower orbital which is compensated by electrons of higher energy. This excess energy is either emitted as characteristic X-Ray or used to eject an electron of the outer orbital. [25]

According to the alloys used in the thermoelements, thermocouples have a distinct name (type). In our experiment a B type thermocouple was responsible for providing the necessary feedback to the furnace power supply and two C-type thermocouples were fabricated for the temperature profile acquisition (see below for more details).

2.3.3   Directional Solidification (DS) and Vertical Gradient Freeze (VGF)

In most modern industrial applications, multi-Si is grown in the same crucible where it is melted, with a technique called Directional Solidification (DS). In this growth method, a SiO_2 crucible coated with silicon nitride (Si_3N_4) is filled with Solar Grade polysilicon (feedstock) as well as the doping element (commonly Boron or Phosphorus). The crucible is then placed in the furnace, surrounded by a graphite case. Afterwards, a pump is used to create a vacuum of $1 \cdot 10^{-2}$ mBar in the furnace. Finally, the pump is shut down and the chamber is filled with an inert gas, most commonly argon, of constant flow in order for vaporized elements to be removed.

Inside the furnace (figure 2.13), heating is achieved through induction. A current flows across a coil, causing the heating of a graphite shield that surrounds the crucible. The heat emitted from the graphite is responsible for warming up the silicon until it is melted, keep its
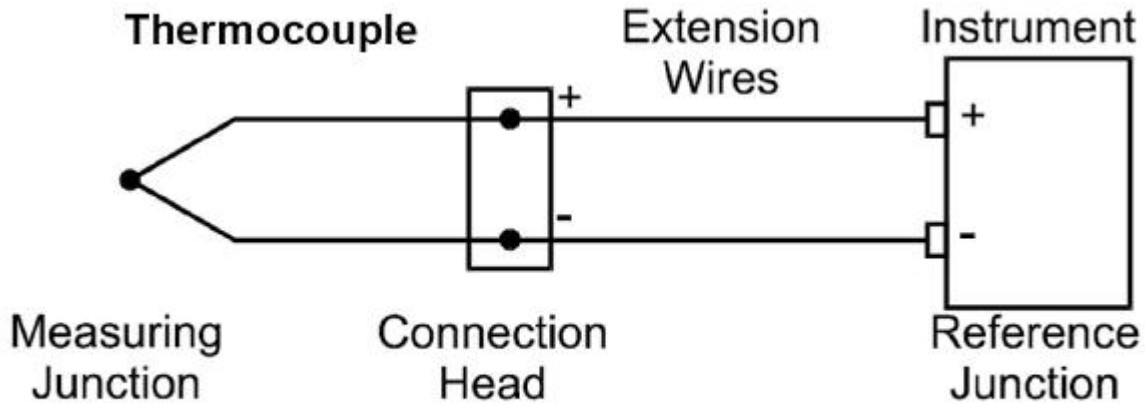
Figure 2.12: Schematic of a Thermocouple

temperature stabilized for a certain period and, finally, cool it down until it completely solidifies and reaches room temperature. A thermocouple measures the temperature in the furnace and provides feedback to the power supply in order to achieve the wanted temperature. In our experiment, two more thermocouples were placed at the top and bottom of the crucible to provide a more accurate temperature profile at those specific points. During the solidification phase, the bottom of the crucible is constantly at a lower temperature than the upper part. As a result, heat is emitted from below to the ambient and solidification proceeds upwards. Because there is always a temperature difference along the height of the silicon, this method of DS is called Vertical Gradient Freeze (VGF).

Ideally, the solid-liquid interface is planar. This requires very good insulation at the sides of the crucible and is achieved by the same graphite shield which is used for heating.

2.3.4 Four point Probe Resistivity Measurements

This is a very simple technique to crudely measure the resistivity of semiconductor samples. A small and known current (I) passes through the two outer probes (see Fig. 2.14). By measuring the voltage (V) between the two inner probes, the resistivity of the sample (ρ) can be calculated using the formula (for bulk samples):
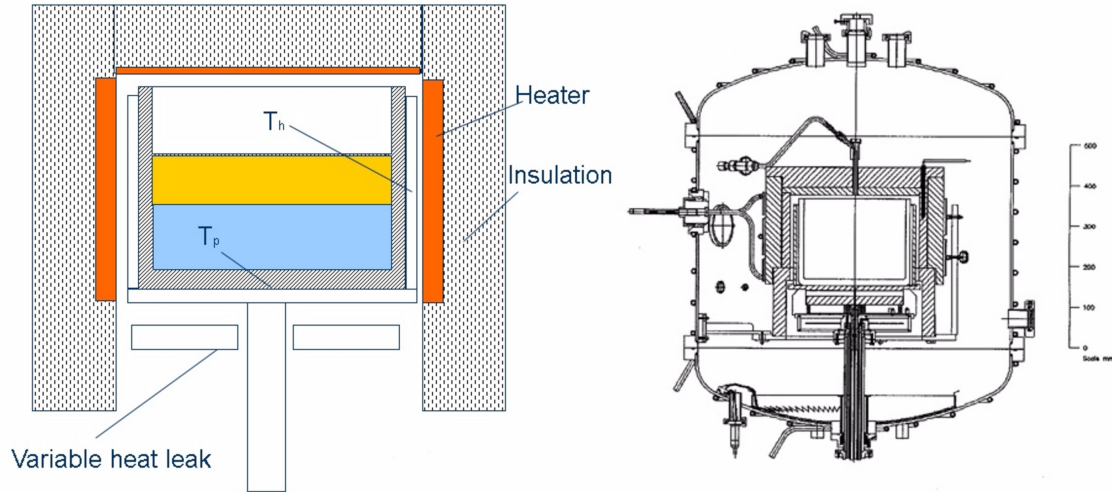
Figure 2.13: Schematic of the Vertical Gradient Freeze Crystallox furnace

$$\rho = \frac{2\pi s V}{I} \tag{2.8}$$

where s is the distance between the probes (assuming equal distance between them).

As doping concentration, N_d, depends on the position in the ingot, it can be identified using the formula:

$$\rho = \frac{1}{\sigma} \tag{2.9}$$

where σ is the conductivity of the sample
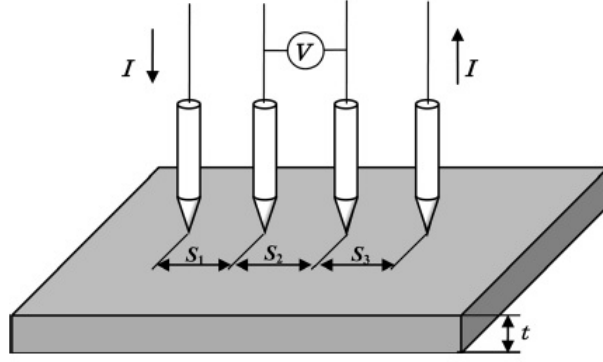
$$\sigma = q\mu_n N_A \tag{2.10}$$

Figure 2.14: Electrical resistivity measurement of semiconductor surface using four-point probe method. [26]

2.3.5 Minority Carrier Lifetime Measurement

When a semiconductor material such as silicon is exposed to light, electrons are excited from the valence to the conduction band, leaving empty states (holes) behind. Depending on the main dopant we have introduced to the semiconductor, we define minority carriers as electrons for p-type and holes for n-type material. Excited minority carriers have an average time to be collected before they recombine and this lifespan is called minority carrier lifetime. This is one of the most important parameters upon characterization of semiconductor materials. Minority carrier lifetime depends on many recombination mechanisms such as radiative recombination, Auger recombination, Shockley-Read-Hall (SRH) recombination, also known as recombination through traps, and surface recombination [22]. Since recombination can occur both in the bulk material and on the surface, we can define the effective carrier lifetime as:

$$\frac{1}{\tau_{eff}} = \frac{1}{\tau_{bulk}} + \frac{1}{\tau_{surf}} = \left(\frac{1}{\tau_{rad}} + \frac{1}{\tau_{Aug}} + \frac{1}{\tau_{SRH}} \right) + \frac{1}{\tau_{surf}} \qquad (2.11)$$

As shown in equation 2.11, the bulk lifetime includes the radiative lifetime, τ_{rad}, the Auger lifetime, τ_{Aug} and the Shockley-Read-Hall lifetime, τ_{SRH}. Surface recombination occurs due to discontinuities of the crystal lattice on the surface. There, missing Si atoms (also called dangling bonds) give rise to a spectrum of allowed states in the silicon bandgap. However, those surface discontinuities can be eliminated by hydrogen through a process called surface passivation.

For indirect bandgap semiconductors such as Si, radiative recombination is extremely rare; for this reason, it can be neglected. In addition, Auger lifetime can be calculated by using simulations (a model has been suggested by Schmidt et al.[27]). On the contrary, SRH lifetime highly depends on the crystal quality and is difficult to calculate through simulations. Therefore, it has to be experimentally investigated.

Quasi Steady State Photoconductance - QSSPC

The first technique that was used in this project is called Quasi Steady State Photoconductance (QSSPC). It is a widely employed method for fast measurements of bulk minority carrier lifetime with relatively low resolution (around 18mm depending on the trap density in the material). A semiconductor block or wafer is illuminated by a long, compared to the carrier lifetime, slowly-decaying light pulse. This allows the excess carriers to be, practically, in steady-state since the generation and recombination rates are balanced (hence the name of the method). The excess electron-hole pairs that are generated, Δn, proportionally increase the material's conductance. A coil, inductively coupled to the charge in the semiconductor, can then measure this excess photoconductance for each time and simultaneously, a sensor measures the intensity of the flash pulse. The sample conductance is converted into the average excess carrier density, Δn, and the measured pulse intensity into the generation rate of electron-hole pairs, G, for each time. Finally, lifetime τ_{bulk} is calculated as a function of excess carrier density via:

$$\tau_{bulk} = \frac{\Delta n}{G} \tag{2.12}$$

Microwave Photoconductance Decay (μW-PCD)

This is another, widely employed, technique for measuring the effective minority carrier lifetime. An infrared (λ=904nm) laser pulse excites free electron-hole pairs which alter the conductivity of the material. After excitation, free carriers recombine, decreasing the sample's conductivity until it reaches equilibrium once again. Conductivity affects the semiconductor's reflectivity at microwave wavelengths. So, it can be monitored by measuring the reflected microwave

power as a function of time. The measured reflectivity resembles an exponential decay and it can be fitted with a curve so that the time constant provides the effective lifetime in this specific position of the sample.
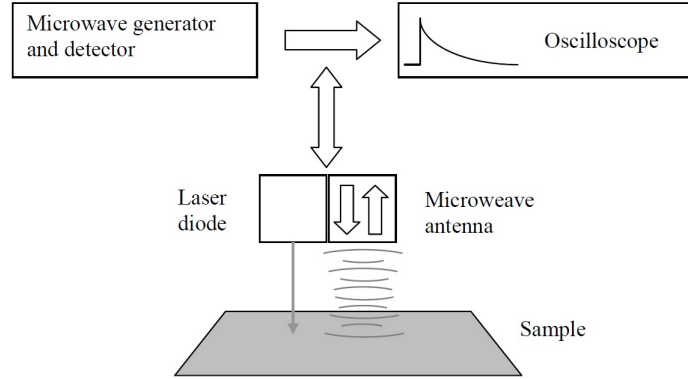

Figure 2.15: Schematic of a μW-PCD setup [28]

2.3.6 Fourier Transform Infrared Spectroscopy (FTIR)

Fourier transform infrared spectroscopy is a fast, non-destructive and accurate chemical analysis method. It can give both qualitative and quantitative results on a wide variety of materials. Its working principle is based on the vibrational modes of different chemical bonds. When a chemical bond is exposed to radiation with the same frequency as the difference between its ground and excited state, it can be promoted to this state absorbing a portion of the initial light pulse. Since pure silicon is transparent to the wavelengths used during FTIR, the absorbance of infrared light, plotted versus the wavenumber of the radiation, can be used to calculate the concentration of specific elements forming the chemical bonds. Downward peaks on the plot suggest absorption at specific wavenumbers which constitute the fingerprints of those bonds.

FTIR is widely used in silicon characterization to identify interstitial oxygen (O_i) and substitutional carbon (C_s) whose absorption peaks lie at 1107 cm^{-1} and 605 cm^{-1}, respectively. A typical absorption spectrum of silicon is shown in figure 2.16. For calculating the concentrations quantitatively, the peak heights relative to the baseline are measured and then multiplied by calibration factors based on specific international standards. In our case the ASTM standards F1188-93a and F1391-93 for (O_i) and (C_s), respectively, were used.
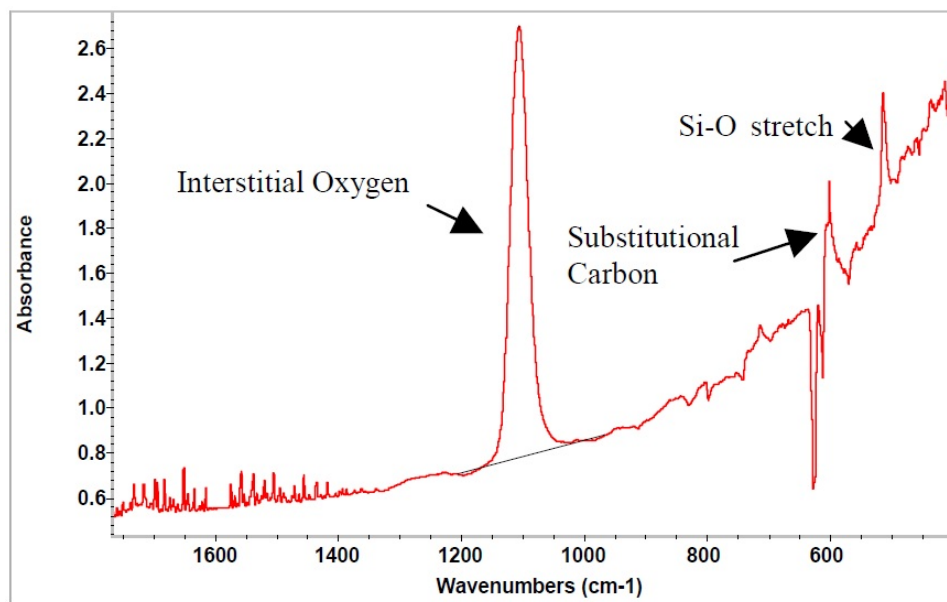
Figure 2.16: Absorption peaks for interstitial oxygen and substitutional carbon in crystalline silicon [29]

Chapter 3

Experimental Procedure and Equipment

Our study involved four experimental parts:

1. Heat treatment of small samples to investigate oxidation effect on porosity and formation of oxynitride layer.

2. Heat treatment and coating of small Si_3N_4 crucibles

3. Casting of silicon ingots

4. Sample Characterization

3.1 Sample and apparatus preparation

In this section, the process of sample preparation as well as thermocouple fabrication are described.

3.1.1 Si_3N_4 samples for electron microscopy

For this experiment, pieces of Si_3N_4 with dimensions 10mm x 10mm x 4mm were ground and roughly polished with silicon carbide sandpapers of average particle diameter 125μm according to FEPA standards. They were heat treated in the presence of oxygen for different durations and temperatures, as illustrated in table 3.1.1.

Warm up Time (h)	Holding Time (h)	Temp.(^oC)
8	12	1200
8	24	1200
8	12	1400
8	24	1400
10	12	1600
10	24	1600

Table 3.1: SEM sample Preparation

After being thermally treated, the samples destined for SEM measurements were dipped in epoxy resin and their cross section was polished up to 1μm with diamond particles. Since Si_3N_4 is a non conductive material it was necessary for the samples to be wrapped around aluminium foil and carbon coated. Finally, they were left overnight in a warm chamber at 70^oC to completely dry and get degassified.

3.1.2 Crucible Preparation and Feedstock

The Si_3N_4 crucibles were fabricated by Steuler Solar Advanced Ceramics through a slip-casting process that involves silicon powder which then goes into a nitridation process at high temperatures until a final silicon nitride product is achieved. The crucibles that were examined had a high concentration of metallic impurities. Specifically, iron and aluminium concentrations were provided by Steuler and they were 380ppmw and 960ppmw respectively. These high values were expected to affect the final product's quality even though coating acts as a diffusion barrier to some extent. Both cylindrical and conical crucibles were tested. The cylindrical crucible had a height of 9cm and an outer diameter of 10cm and the conical one had top diameter of 9.0 cm, a bottom diameter of 6.5 cm and a height of 12.2 cm.

Firstly, four cylindrical crucibles were prepared for solidification. They were all left overnight in a warm chamber at 150^oC for drying and degassing. Afterwards each one was heat treated at a different temperature under atmospheric air. Two crucibles were heated up to 1200^oC, one up to 1400^oC and one up to 1600^oC. This step had a binary purpose: first of all, to create the necessary oxidized layer and SiO_2 crust needed for non-wettability properties, and, secondly, to block the pore channels and reduce diffusivity of impurities into the silicon ingot. However,
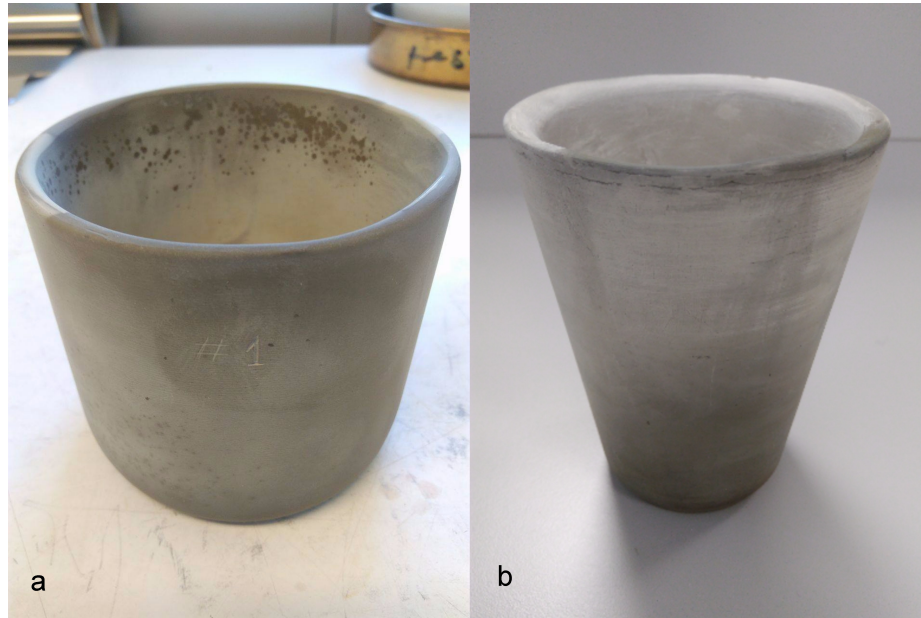
Figure 3.1: Cylindrical (a) and conical (b) silicon nitride crucibles used for directional solidification

during thermal treatment they were all damaged externally either by forming cracks (fig. 3.2 (a)) or by exfoliation of the outer part (fig. 3.2 (b)). Finally, two of the crucibles broke completely; one during the initial heat treatment at 1600°C and another one during Si_3N_4 coating (fig. 3.2 (c))

Figure 3.2: Cracks and outer surface flaking of cylindrical crucibles after heat treatment

One possible explanation to this behaviour is that water was still trapped in the pores of the crucibles and caused violent expansion upon heating to very high temperatures. Another possibility is that errors in the casting process had created areas with high inhomogeneity which behaved differently during heat treatment. The cylindrical crucibles were discarded and only the conical ones were tested afterwards.

The next attempt involved the preparation of the conical crucibles. Four similar crucibles

Coating	Method
Si_3N_4 powder	Warming up to 450^oC Spray coating with Si_3N_4 solution Heat treatment at 1100^oC for 4 hours Cooling down to 700^oC and keeping for 2 hours
Colloidal Silica	95% Si_3N_4 mixed with 5% SiO_2 solution Same process as above
Barium Oxide and Si_3N_4 powder	Intermediate BaO coating as described in 2.1.4 Normal Si_3N_4 coating on top
Uncoated	-

Table 3.2: Crucible coating parameters

were left overnight at 150^oC for drying and degassing. According to the EDS measurements, it was discovered that maximum oxidation was achieved when heat treatment was done at 1200^oC. Consequently, they were heated at 1200^oC for twelve hours in the presence of atmospheric air. The warm-up rate was 150^oC/h. After heat treatment three of them were coated and one was left uncoated according to table 3.2.

The crucible that was firstly treated with BaO had to be coated twice afterwards because the first attempt failed (see fig.3.3a). A possible reason for this could be that a thick layer of $Ba(OH)_2$ powder that had not been absorbed by the crucible prevented the Si_3N_4 coating from sticking properly to the substrate. In addition, at the bottom of the crucible, some reaction had caused the color to change to green (fig. 3.3b).

The final step of the preparation was filling the crucibles with polysilicon feedstock. A Boron alloy of concentration $1.4E19\frac{atoms}{cm^3}$ was used. In order to achieve the required resistivity of 1 Ohm*cm in the ingot, the alloy was mixed with the polysilicon in a ratio of $\frac{0.12}{100}[wt]$.

3.1.3   Building the Thermocouple

In order to measure the temperature inside the furnace with higher accuracy, two C type thermocouples were fabricated and inserted in the chamber. To prevent the wires from touching each other and causing a short circuit, they were inserted in a ceramic tube (see fig. 3.4a).

The next step required building a feed through port to transfer the signal out of the furnace without causing interference and disturbing the vacuum. Therefore, two compensation cables were passed through an aluminium tube which was then filled with epoxy resin and left
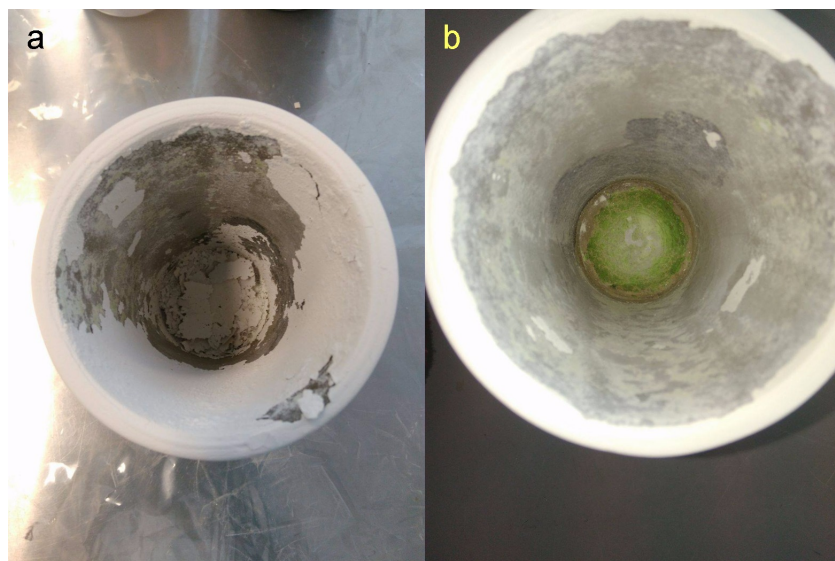
Figure 3.3: (a) Peeled-off Si_3N_4 coating after treatment with $Ba(OH)_2$. (b) Change of color after reaction

overnight to dry. Two connectors were mounted on the compensation cable ends afterwards and the feedthrough port was mounted on the furnace chamber (fig 3.4b).

3.1.4   Four Point Probe and QSSPC

One bulk sample (1cm thickness) from each of the three ingots that were characterized was ground and roughly polished on one side using 80 to 1200 grit SiC paper.

3.1.5   FTIR

One slice of 2mm thickness was sliced from each ingot by using a diamond saw. They were all mechanically polished from 80 grit SiC paper up to 1μm diamond particles (mirror-like surface) on both sides.

3.2   Solidification

Given the size of the crucibles we used, the nature of our experiments was unprecedented. Therefore, we had to develop and implement a whole new technique in order to customize the current method and make it suit our facts.
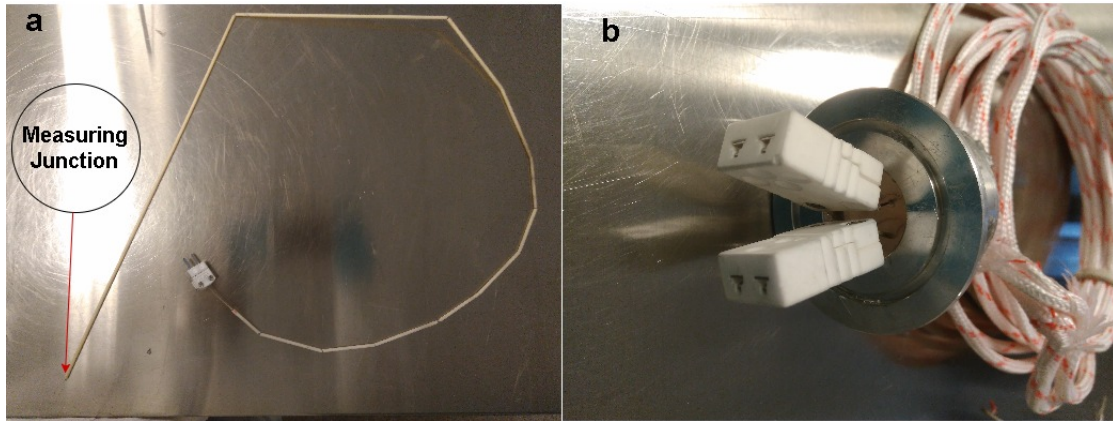
Figure 3.4:   (a) A C-type thermocouple enclosed in ceramic tube. (b) Feedthrough port with connectors and compensation cable

The four crucibles that were prepared were inserted into the Crystalox furnace (see fig. 3.5). For safety reasons, but also for higher temperature homogeneity, they were placed inside a large quartz crucible as can be seen in the same picture. This specific furnace is programmed to create large silicon ingots in such crucibles. Therefore, a graphite felt insulator of 1cm thickness was placed at the bottom of the large crucible to create an effective thermal gradient between the top and the bottom of the crucible.
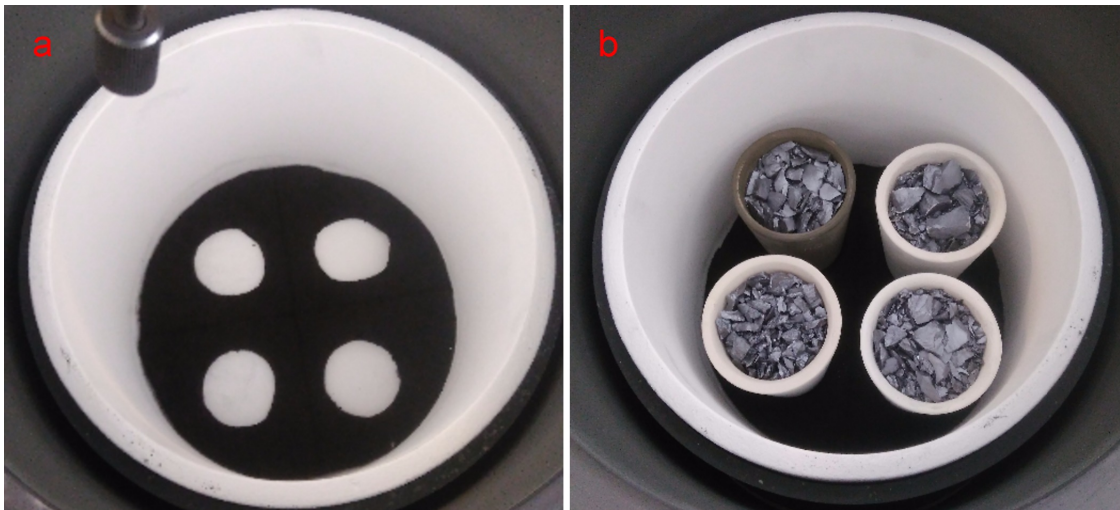

Figure 3.5: a) 1cm of graphite felt placed at the bottom of a large quartz crucible; b) four crucibles filled with polysilicon feedstock are added, fitting in the felt holes.

The first step was creating vacuum inside the furnace. When the pressure had reached 0.08 mbar the warming up phase started. During this process, gasses and volatiles that had been

adhered to the furnace surface evaporated and were pumped out of the chamber. The second phase started when the temperature had reached 900^oC. Then, the pump was turned off and a valve was opened to let argon at a constant flow inside the furnace. The pressure reached 1atm again. The warming up process continued until the temperature reached 1500^oC, which is above the melting point of Si. In order to ensure complete melting, the system was kept stable at this temperature for 5.5 hours. Afterwards, a heat leakage valve opened from below and the solidification process started.

Since the program was set to keep a specific temperature profile, the power supply needed to function accordingly in order to achieve the wanted result. This is very important in order to acquire information regarding the solidification process. As long as a material changes phase from liquid to solid, heat is emitted into the environment which means that there is a lower need for external power to meet the temperature needs. However, when the solidification is complete, a slight rise in the power supply is necessary to keep the temperature slope in the controller. The reason is that when the solidification is finished there is no latent heat from the solidification. This phenomenon can be observed in graph 3.6 about 8 hours after the solidification process started.

Finally, the system was left to cool down until it reached room temperature and the ingots were removed from the furnace. An overview of the temperature levels but also the power as a function of time is given in graph 3.6.

Another important observation we can make is that the two C-type thermocouples we fabricated show a much lower temperature than the actual one (around 500^oC less). This divergence was caused by a very strong coupling between the induction heating system and the thermocouples. As can be seen in the graph, every change in the power supply affects the temperature signal. However, the most important information acquired from this data is that during solidification there is always a 25-40^oC difference from the top to the bottom of the crucibles, thus ensuring directional solidification.
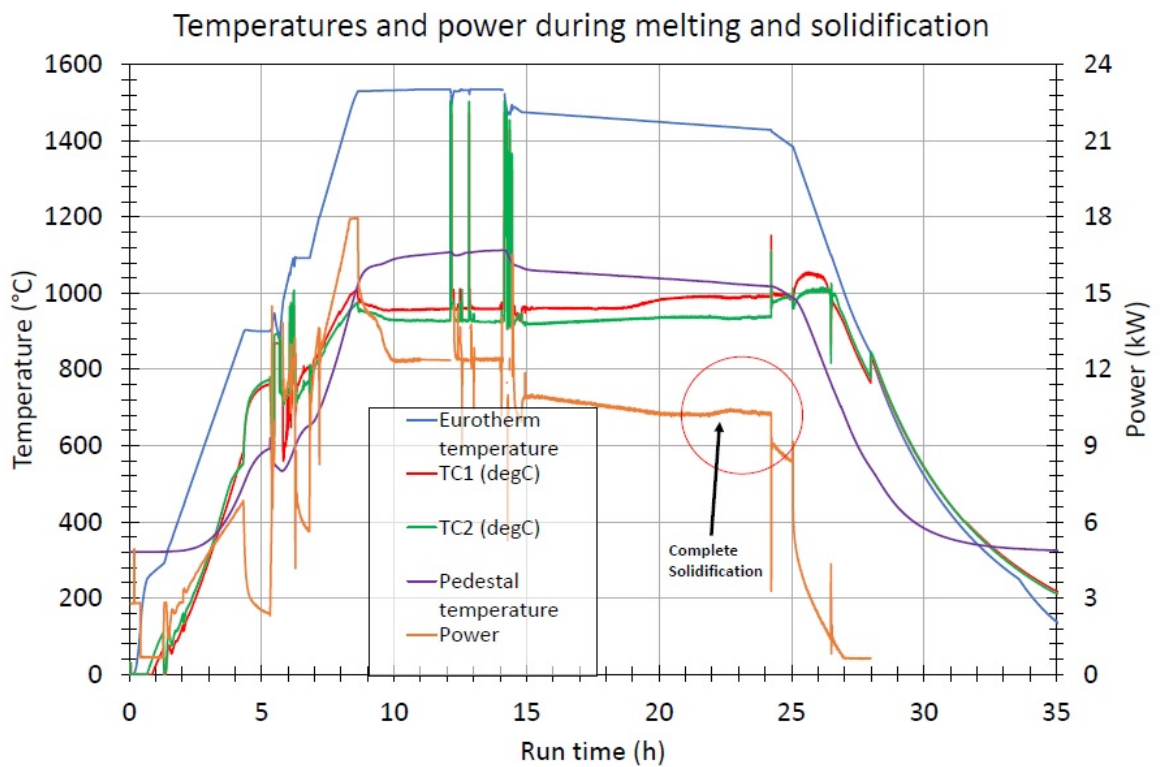
Figure 3.6: Temperature and power levels during the solidification process

Chapter 4

Results and Discussion

4.1 Mass gain

A crude but often useful way to identify the change in elemental structure of specimens after heat treatment is by measuring the change in mass. This process can only give qualitative results because the chemical reactions during calcination cannot be precisely described. According to our predictions based on the study by Ogbuji and Jayne [7], we expect the replacement of nitrogen by the slightly heavier oxygen. However, we cannot exclude the possibility of interstitial oxygen which would further cause an increase of the samples' mass. The weight of both small samples and crucibles was measured before and after heat treatment. The percentage change in mass after heat treatment is shown in table 4.1.

Those results were in accordance with the theoretical expectations found in the literature [9]. As expected, oxidation in higher temperatures reaches a maximum much faster and thermal annealing for longer exposure times does not play any role. Moreover, the total amount of oxidation is lower as the protective SiO_2 that is created faster prohibits any further diffusion of oxygen into the sample pores. Finally, the samples that were treated at 1600^oC showed signs of bubble creation and surface cracking (see figure 4.1), something that suggests the unsuitability of this temperature for any further investigations.

Kind of Sample	Thermal Treatment	Average mass gain	final condition
Small Sample	12h 1200°C	3.42%	stable
Small Sample	24h 1200°C	3.70%	stable
Small Sample	12h 1400°C	2.01%	stable
Small Sample	24h 1400°C	2.01%	stable
Small Sample	12h 1600°C	1.83%	small cracks
Small Sample	24h 1600°C	1.37%	small cracks
Conical Crucibles	12h 1200°C	2.32%	stable
Cylindrical Crucibles	12h 1200°C	1.83%	Broke during coating
Cylindrical Crucibles	12h 1400°C	-	Broke during heat treatment

Table 4.1: Difference by percentage in samples' weight. Higher mass gain in lower temperatures suggests that pore channels get sealed by oxygen faster as temperature increases.

4.2 SEM

In our experiments with the electron microscope, the goal was to characterize the micro structure of silicon nitride after heat treatment and identify the depth and magnitude of oxidation. A low energy primary electron beam (5kV) was used in order to achieve high surface imaging resolution. The samples were investigated through a secondary electron detector and showed the presence of a brittle material near the edges after thermal treatment (see figure 4.2).

Later investigation with EDS showed that this was a silicon oxide layer as was expected by the literature and previous studies. Moreover, EDS experiments on samples treated at 1400°C revealed a layer of varying thickness (70μm-150μm) directly below the silicon dioxide crust with significantly higher oxygen concentration than the rest of the sample. Finally, comparing the Si_3N_4 samples before and after heat treatment, we can observe that the material's porosity has been reduced to some extent due to oxidation, but the pores have not been completely sealed. This indicates higher chance of wetting during silicon solidification.

Line scans were performed on all samples to investigate the oxidation profile relative to the temperature and duration of heat treatment. The results are illustrated in graph. 4.3.

According to the results, the highest oxidation levels were achieved through heat treatment in low temperature (1200°C). It is also notable that heat treatment in 1400°C and 1600°C caused higher oxidation levels near the edges than the middle of the samples. This was probably caused due to minimization of porosity near the edges through high rate of oxygen absorption.
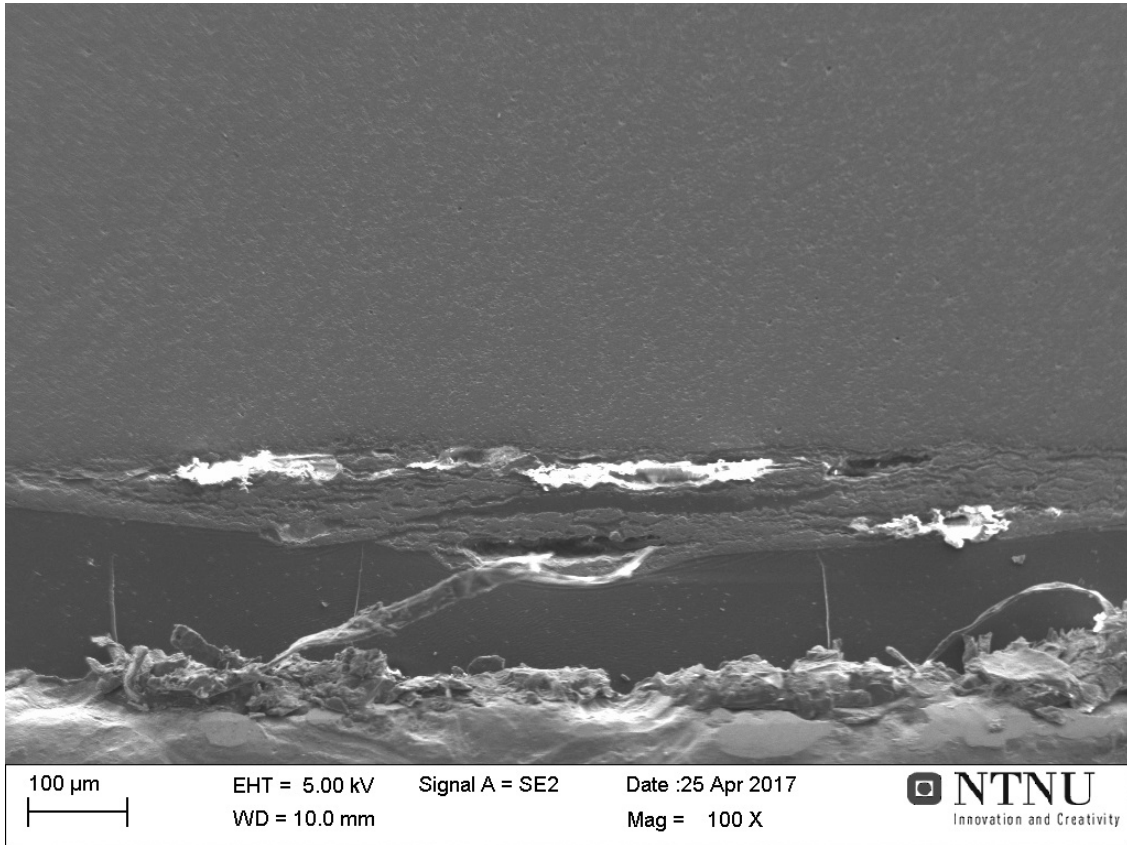
Figure 4.1: SEM image showing the formation of bubble during heat treatment at 1600°C

4.3 Solidification and ingot production

After the furnace had cooled down, it was opened and the four crucibles were removed. The crucible without coating had broken but the silicon ingots seemed to have been successfully grown in all four crucibles. The ingots seemed, at first, attached to the crucibles, which rendered their separation infeasible, leaving cutting the ingots out of the crucibles as the only option. However, during the process of doing so, two out of the four ingots (normal coating and colloidal silica) detached form the crucibles on their own. The ingot grown in the crucible with a mix of colloidal silica and Si_3N_4 coating (4.4a) was cleaner than the rest, a fact which suggests that it had, indeed, enhanced its mechanical stability.

One more ingot, the one grown in the BaO coated crucible (4.4d), was also released after it was cut in half. It was then revealed that due to improper coating at the bottom of the crucible, a small part of the ingot was in direct touch with the Si_3N_4 beneath and had wetted the substrate, which had caused strong sticking (4.4e).
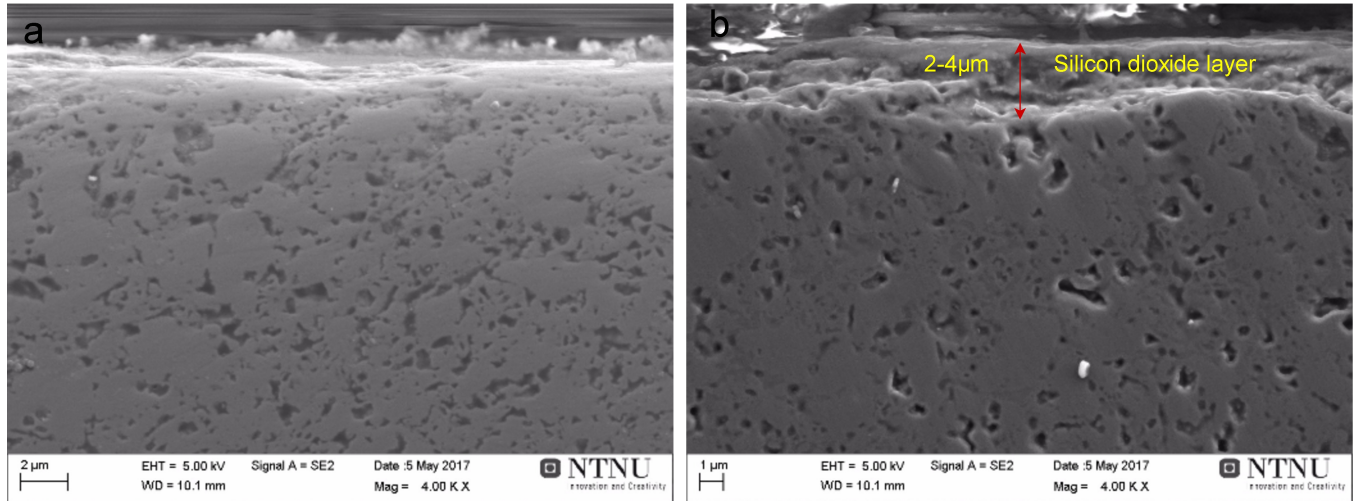
Figure 4.2: Comparison of sample edges before and after thermal treatment at 1200^oC. A brittle silicon oxide layer has been formed on the second sample.

The only ingot to remain attached to the crucible even after cutting was the one grown in the crucible without coating. Excessive wetting had caused deep infiltration of silicon into the Si_3N_4 substrate. In addition, direct contact with the crucible gave rise to large scale bulk defects such as dislocations and voids as seen in figure 4.4c. The ingot was cut using a SiC disc and a small sample was examined with an optical microscope (see fig.4.5). It was revealed that, due to the crucible's porosity, silicon had penetrated the substrate and had caused the formation of a 30μm wide region with excessive wetting of the crucible. Coefficients of thermal expansion differ between Si ($2.6 \cdot 10^{-6}/^OC$) and Si_3N_4 ($3.3 \cdot 10^{-6}/^OC$). In case of such wetting, shrinking during the cool-down phase will cause immense stress between the two materials, resulting in cracks as depicted.

After closer observation, it was seen that the shape of the ingots was not purely conical as expected but their bottom was wider (fig. 4.4a). This deformity was due to the shape of the crucible and had also caused the initial sticking of the ingots.

However, the crucibles showed no other sign of damage (cracking or flaking) after the whole process, something which suggests that they remained mechanically and chemically stable during solidification and they could have likely been reused for more silicon ingot production.
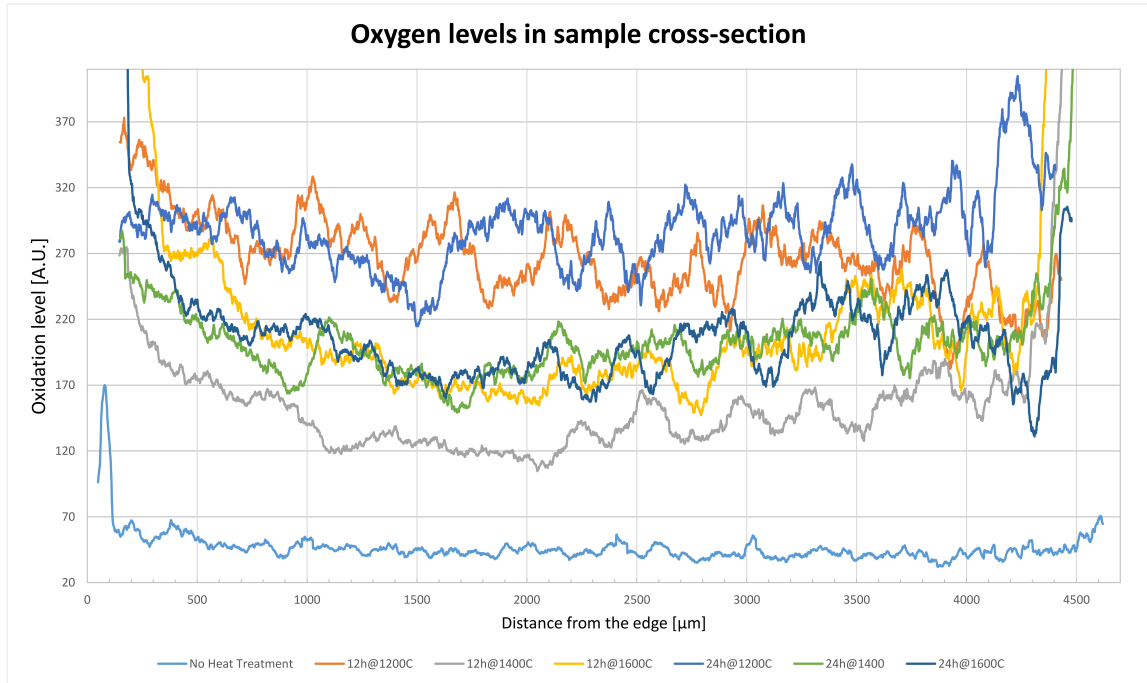
Figure 4.3: EDS line scan showing oxidation levels in all samples

4.4 Resistivity

After the bulk samples had been prepared they were tested with a Jandel RM2 system. The probes in the head that was used had a spacing of s=1.591mm and a constant current of 5mA was induced. Thus, the resistivity of the silicon ingots along the growth axis was acquired and the results are displayed in graph 4.6. For the silicon ingot grown in the crucible with the normal coating, a curve representing the theoretical resistivity from Sheil's equation was also calculated and is shown in the same graph. Experimental values follow Sheil's equation with an exception near the bottom where high resistivity fluctuation is probably caused by bad sample-probe contact.

We can see that the values vary between 0.1-1 Ohm·cm and the resistivity is lower towards the top, something that was expected due to higher concentration of Boron (segregation of impurities to the end). Moreover, the dopant concentration was calculated, using the empirical data from the book of ASTM standards [30]. It was found to be in the range of $10^{16} - 10^{17} \frac{atoms}{cm^3}$ with slight variations among the different ingots and increasing towards the top. The ingot
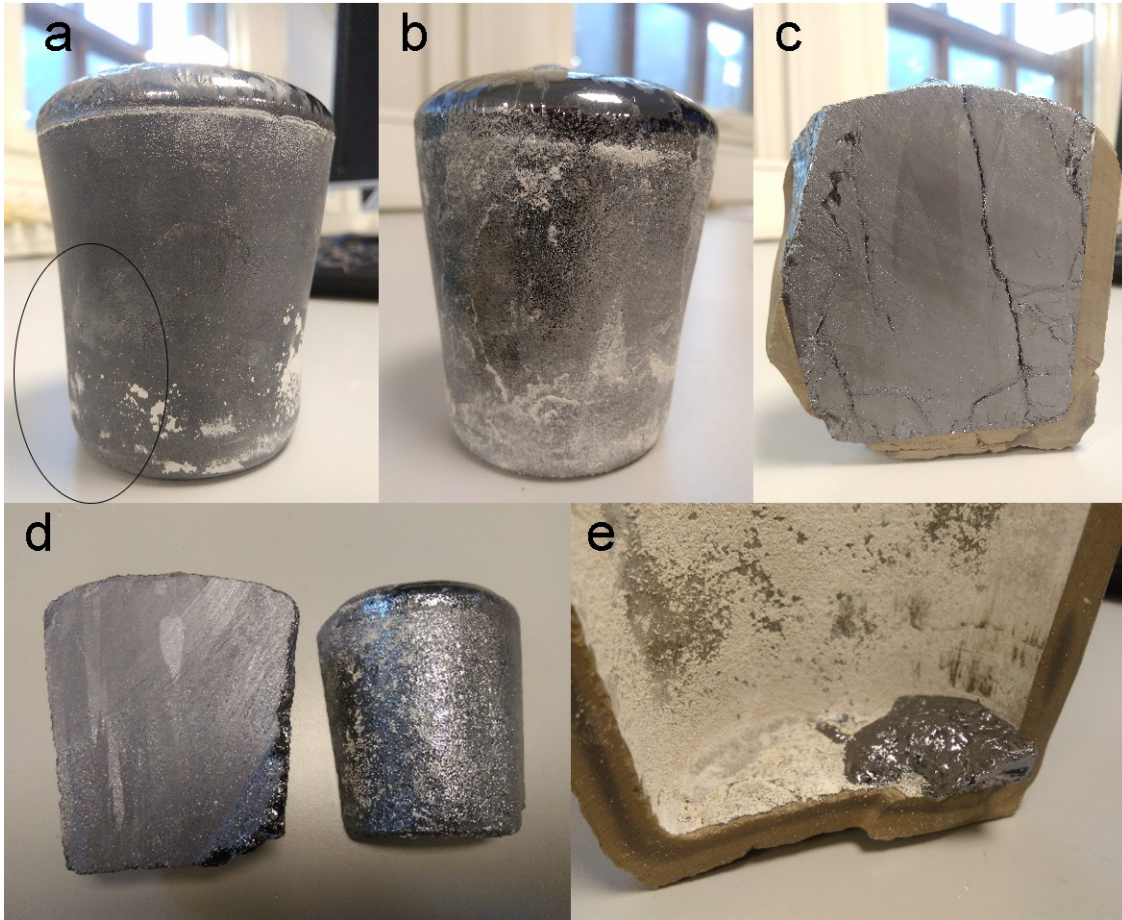
Figure 4.4:   Ingots from all four crucibles: a) colloidal silica-Si_3N_4 mix coating; Here, the non-conical shape of the ingot is clearly seen; b) normal Si_3N_4 coating; c) uncoated crucible; d) BaO intermediate layer; d) sticking of silicon due to improper coating.

grown in the BaO treated crucible showed highly varying signals (3 orders of magnitude difference) between close regions in the ingot. This was probably caused by oxides in the crystal lattice, which caused very high local resistivity. Later, study with FTIR showed that its O_i concentration was more than 3 times higher than the other two samples. Finally, the resistivity of the ingot grown on colloidal silica mix coating is lower than the other two. This could be due to small deviation in the doping concentration but we cannot exclude the possibility that it is also caused by high presence of Al which lies in the same column as boron and can act as p-type dopant.
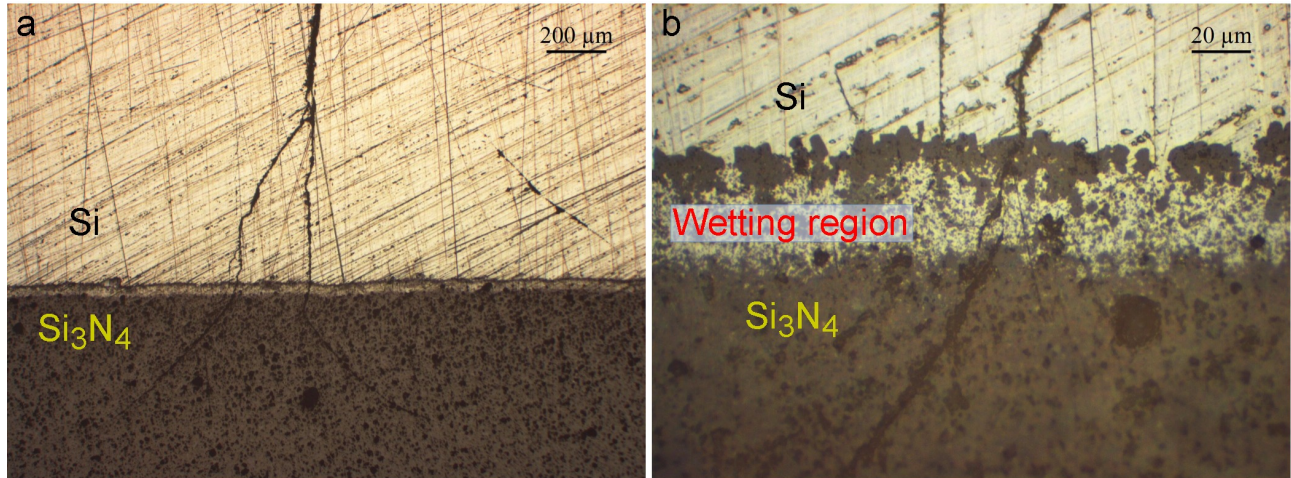
Figure 4.5: Cross-section of the Si-Si_3N_4 interface from the non-coated crucible after solidification: a) excessive wetting resulted in cracking and the formation of defects; b)a 30μm wide wetting region had caused strong sticking

4.5   Minority Carrier Lifetime

The QSSPC measurements were performed on a BCT-300 photoconductance instrument. Lifetimes were measured near the center of each sample to ensure that the coil does not exceed the sample's borders but also because it is the region where lifetime is expected to be the highest. The acquired values are presented in table 4.5.

Type of coating	Average effective lifetime [μs]
Normal Si_3N_4	5.6
Colloidal Silica mix	0
BaO + Si_3N_4	5.8

Table 4.2: Average lifetime measured by the QSSPC method.

It is important to mention, at this point, a trapping phenomenon which can give rise to extraordinarily high lifetime values. When a number of shallow energy levels are present in the band gap, minority carriers are captured and released again, resulting in high lifetimes which need to be taken into consideration. The density of these shallow traps depends on defect density and is expected to rise near the red-zone of the ingot. Since the size of our ingots was so small, accurate measurements of lifetime with QSSPC were almost impossible. Therefore, they were also examined using the μw-PCD method.
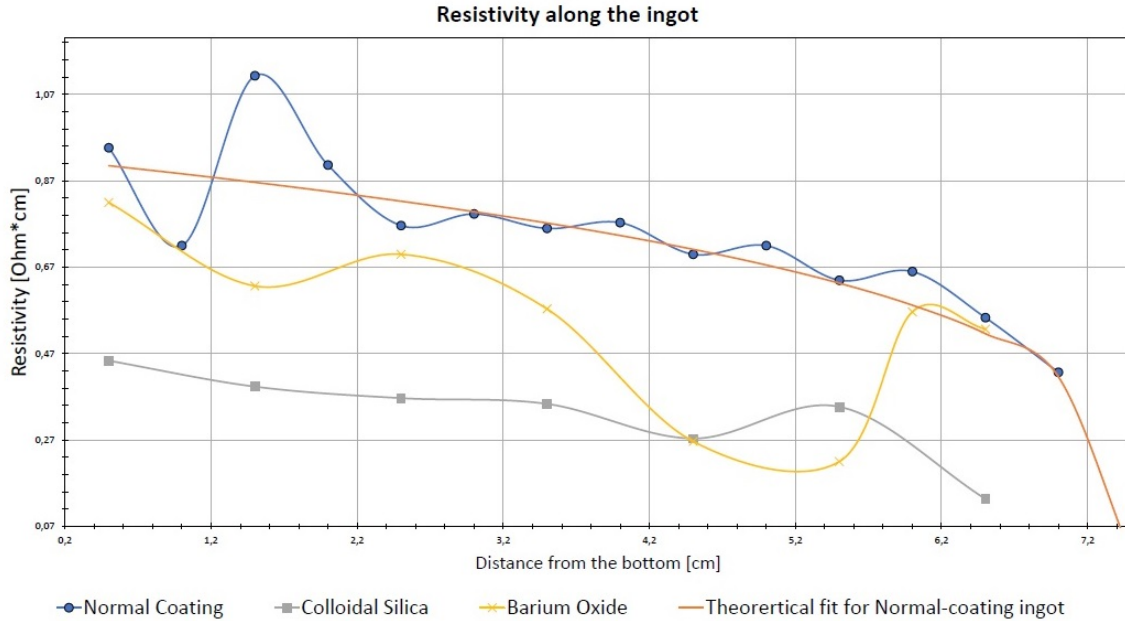
Figure 4.6: Resistivity along the three silicon ingots.

The thickness of our bulk samples was too high to fit in the microwave scanner so, the polished samples that were prepared for the FTIR analysis were examined instead. The sample acquired from the BaO coated crucible represents half of the cross-section of the ingot. As a result, the highest lifetimes are expected at the top left border. An overview of the lifetime mapping is illustrated in fig. 4.7.

The ingot grown on the colloidal Silica mix coating (4.7.b) showed almost no lifetime with both techniques. This was probably caused by metallic impurities introduced in the crucible by the crucible and during feedstock filling. The highest bulk lifetime was acquired from the normal coating ingot and was roughly 5μs. Such low lifetimes were to be expected from small ingots and without any sample passivation. A previous study by Boulfrad et al. [31] on the same furnace showed that the extent of red zone is approximately 2cm. Given the size and contamination of our crucibles, the acquired results were to be expected. On an industrial scale, defects and impurities introduced by the crucible are much lower proportionally and material performance rises rapidly.
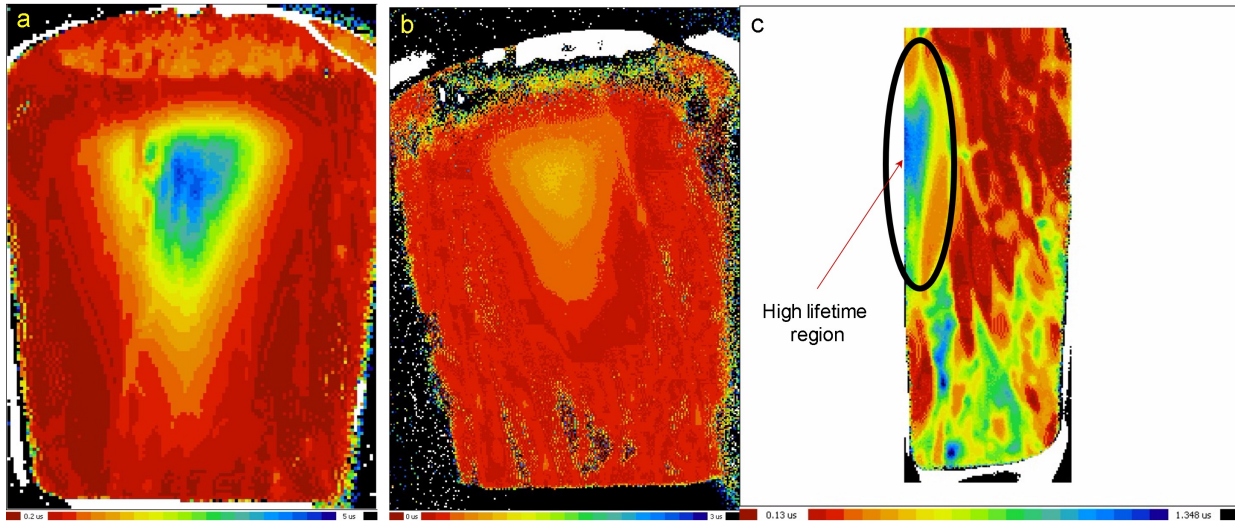
Figure 4.7: Lifetime mapping acquired with μw-PCD: a) Normal Coating; b) Colloidal Silica mix; c)BaO intermediate coating

4.6 Chemical Analysis

The FTIR measurements were performed on a Nicolet 6700 by Thermo Scientific, using a resolution of $4cm^{-1}$ and number of scans, 32. Firstly, a calibration measurement was taken to measure the background concentration of light elements due to the atmosphere. These values are stored and then subtracted from the sample measurements to reassure minimal noise interference from the environment. Afterwards, FTIR measurements were performed near the top and center of each sample, where the lifetime was found to be highest. The qualitative results are presented in graph 4.8.

The presence of both O_i and C_s is confirmed in all samples. However, high impurity concentration near the vibrational mode of C_s in the sample from the colloidal-Si coated crucible has caused extreme noise, thus making the detection of carbon infeasible. We assume that this was caused by the metallic impurities that were also lifetime-killing factors. When impurities cause the light to scatter multiple times within the sample, interference fringes arise. It is also important to note that FTIR only detects vibrations between specific bonds. Therefore, oxygen or carbon grown on precipitates is transparent to this technique and need to be detected with other methods; a possible way could be etching followed by examination with microscope.

The quantitative calculation is an automatized process done by the FTIR software and works as described in chapter 2.3.6. The concentration numbers were given in ppma and were con-
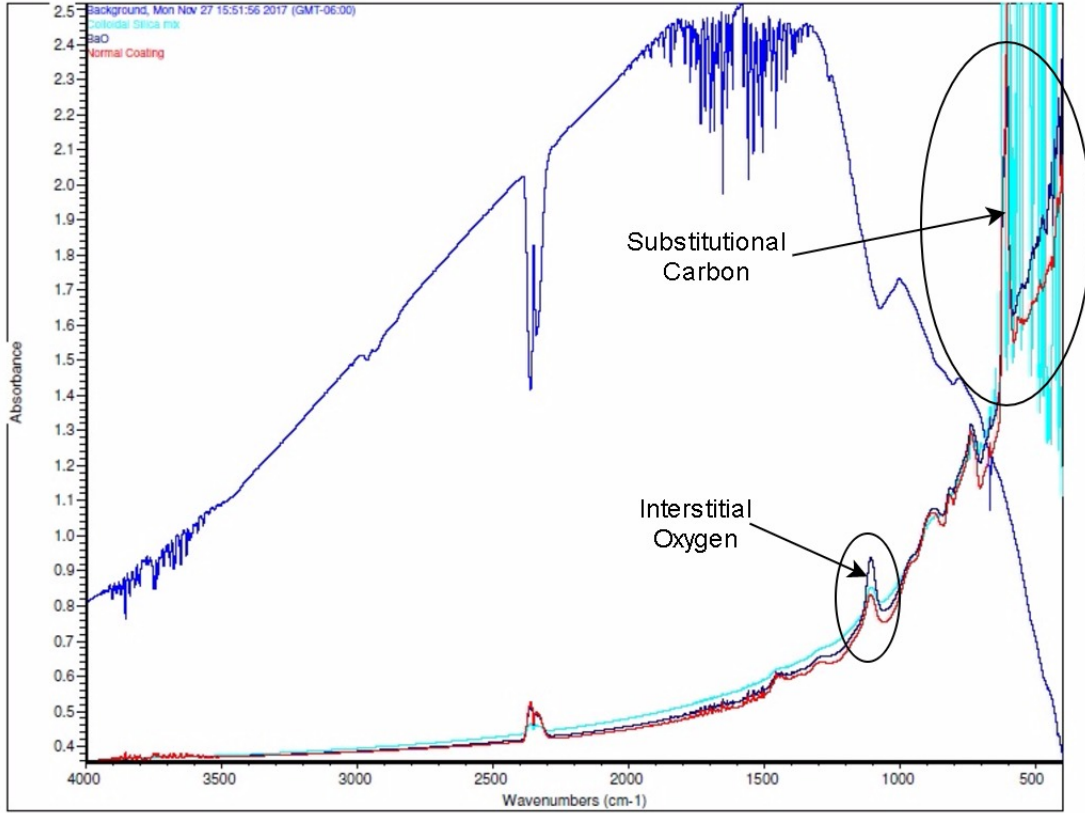
Figure 4.8: Qualitative FTIR results from all samples. High noise-to-signal ratio near the C_s region for the sample from the colloidal-Si coated crucible is probably due to the metallic impurities.

verted into absolute numbers $\left(\dfrac{atoms}{cm^3}\right)$ by using the SEMI AUX022-0611 standards.

Element $\left[10^{17}\dfrac{atoms}{cm^3}\right]$ Type Of Coating	O_i	C_s
Normal Si_3N_4	1.9	6.35
Colloidal Silica mix	0.5	-
BaO + Si_3N_4	5.8	5.9

Table 4.3: Concentration of O_i and C_s measured by FTIR

The acquired results show similar oxygen concentration to the study by Häßler et al. [16] where O_i near the top of the ingot was $2 \cdot 10^{17}\dfrac{atoms}{cm^3}$. In addition, the sample from the colloidal silica mix coating shows about 1/4 less O_i concentration compared to the normal one. This could be due to the enhanced stability of the coating since the oxidized coating has a lower

grade of diffusion into the melt.

Chapter 5

Conclusions and further work

Summarizing, Si_3N_4 crucibles are a very promising alternative to the industrial standard SiO_2 ones. Even after multiple heat treatments in very high temperatures they showed mechanical durability and were able to grow ingots of high quality relative to their size. The initial purity of the Si_3N_4 powder that is used to cast the crucibles is of high importance; impurities, especially metallic ones can completely destroy a semiconductor. Therefore, they need to be minimized because they can diffuse into the silicon even through the coating. However, non-disposable crucibles can be expected to perform better after each use, since they get cleaner. Shape and size are also important. In our case, they had to be destroyed to release the ingots, but on industrial levels, where they need to follow the approved standards, they can be optimized to grow high quality silicon ingots that can easily be detached.

Coating is still inevitable and plays a key role in the outcome. Out of the three coating methods that were tested, the colloidal silica mix was the closest one to the ideal behaviour of coatings. It interacted the least with the silicon and could also have been the reason for low oxygen content in the ingot. Unfortunately, high concentration of metals from the crucible didn't allow for lifetime measurements which need to be performed in further studies.

The BaO intermediate layer did not prevent oxygen and carbon from diffusing into the molten silicon. In addition, the four point probe measurements showed local resistivity with values up to 3 orders of magnitude difference between nearby locations (approximately 1mm distance). This anomaly persisted even after better polishing, something that excludes the possibility of bad sample-probe contact. In my opinion, this was caused by high concentration of oxides that

could have been formed because of the BaO.

Further research that includes chemical analysis for metallic impurities needs to be conducted. Since the initial concentration of metals in the crucible is known, such a study can show the effect of oxidation and coating as a diffusion barrier. Another parameter that needs to be further studied is the grain characteristics during solidification. Identifying grain size and orientation could reveal many details of the Si-crucible interaction and the effect of different coatings. Finally, the transition from lab to industrial scale requires many identical tests in order to ensure statistical homogeneity of results. Therefore, future work should include the same process with slight variations for optimization purposes.

Bibliography

[1] Fraunhofer ISE. ©Fraunhofer ISE: Photovoltaics Report, updated: 17 November 2016. Technical Report November, 2016.

[2] Semi Pv Group. International Technology Roadmap for Photovoltaic—. *Itrpv*, (March):1–37, 2017.

[3] C Kittel. *Introduction to Solid State Physics*, volume 8th editio. 2004.

[4] Paul A. Basore. Defining terms for crystalline silicon solar cells. *Progress in Photovoltaics: Research and Applications*, 2(2):177–179, 1994.

[5] Christiana Honsberg and Stuart Bowden. Multi Crystalline Silicon, 2017.

[6] M. Gunzburger, E. Ozugurlu, J. Turner, and H. Zhang. Controlling transport phenomena in the Czochralski crystal growth process. *Journal of Crystal Growth*, 234(1):47–62, 2002.

[7] L. U. T. Ogbuji. Mechanism of Incipient Oxidation of Bulk Chemical Vapor Deposited Si[sub 3]N[sub 4]. *Journal of The Electrochemical Society*, 140(3):759, 1993.

[8] Honghua Du. Thermodynamics of the Si-N-O System and Kinetic Modeling of Oxidation of Si[sub 3]N[sub 4]. *Journal of The Electrochemical Society*, 136(11):3210, 1989.

[9] F. PORZ and F. Thummler. Oxidation mechanism of porous silicon nitride. *Journal of Materials Science*, 19:1283–1295, 1984.

[10] J G Li and H Hausner. Influence of Oxygen Partial Pressure on the Wetting Behaviour of Silicon Nitride by Molten Silicon. 9:101–105, 1992.

[11] Ingvild Brynjulfsen, Astrid Bakken, Merete Tangstad, and Lars Arnberg. Influence of oxidation on the wetting behavior of liquid silicon on Si 3 N 4 -coated substrates. *Journal of Crystal Growth*, 312(16-17):2404–2410, 2010.

[12] M Sayuti, S Sulaiman, T R Vijayaram, B T H T Baharudin, and M K a Arifin. Manufacturing and Properties of Quartz (SiO 2) Particulate Reinforced Al-11 . 8 % Si Matrix Composites. *Matrix*, 2012.

[13] Silicon Nitride Crucible Coatings for Photovoltaic Cell Manufacturing. H.C Stark:1–6, 2014.

[14] G. Rancoule. Crucible for the crystallization of silicon and process for making the same, October 30 2012. US Patent 8,298,333.

[15] C. C. Hsieh, A. Lan, C. Hsu, and C. W. Lan. Improvement of multi-crystalline silicon ingot growth by using diffusion barriers. *Journal of Crystal Growth*, 401:727–731, 2014.

[16] C. Häßler, H. U. Hofs, W. Koch, G. Stollwerck, A. Müller, D. Karg, and G. Pensl. Formation and annihilation of oxygen donors in multicrystalline silicon for solar cells. *Materials Science and Engineering B: Solid-State Materials for Advanced Technology*, 71:39–46, 2000.

[17] Arjan Çiftja. *Solar silicon refining; Inclusions, settling, filtration, wetting.* PhD thesis, 2009.

[18] Rannveig Kvande. *Incorporation of impurities during directional solidification of multicrystalline silicon for solar cells.* PhD thesis, NTNU, 2008.

[19] W. Von Ammon, R. Hölzl, J. Virbulis, E. Dornberger, R. Schmolke, and D. Gräf. The impact of nitrogen on the defect aggregation in silicon. *Journal of Crystal Growth*, 226(1):19–30, 2001.

[20] Song Zhang, Mari Juel, Eivind Johannes Vrelid, and Gabriella Tranell. Investigating the effect of carbon on oxygen behavior in n-type Czochralski silicon for PV application. *Journal of Crystal Growth*, 411:63–70, 2015.

[21] R. Kvande, L. J. Geerligs, G. Coletti, L. Arnberg, M. Di Sabatino, E. J. Øvrelid, and C. C. Swanson. Distribution of iron in multicrystalline silicon ingots. *Journal of Applied Physics*, 104(6), 2008.

[22] Guilherme Gaspar. N-type Czochralski silicon solidification. (March), 2016.

[23] Joseph I. Goldstein, Dale E. Newbury, Patrick. Echlin, David C. Joy, Charles E. Lyman, Eric. Lifshin, Linda. Sawyer, and Joseph R. Michael. *Scanning Electron Microscopy and X-ray Microanalysis.* Springer US, 2003.

[24] Jim Mazzullo. *Backscattered Scanning Electron Microscopy and Image Analysis of Sediments and Sedimentary Rocks*, volume 80. 1999.

[25] Matthew Dewar. Characterization and Evaluation of Aged 20Cr32Ni1Nb Stainless Steels. page 235, 2013.

[26] Akira Shimamoto, Keitaro Yamashita, Hirofumi Inoue, Sung-Mo Yang, Masahiro Iwata, and Natsuko Ike. A Nondestructive Evaluation Method: Measuring the Fixed Strength of Spot-Welded Joint Points by Surface Electrical Resistivity. *Journal of Pressure Vessel Technology*, 135(2):0215011–215017, 2013.

[27] Jan Schmidt, Mark Kerr, and Pietro P. Altermatt. Coulomb-enhanced Auger recombination in crystalline silicon at intermediate and high injection densities. *http://oasc12039.247realmedia.com/RealMedia/ads/click_lx.ads/www.aip.org/pt/adcenter/pdfcover_test/L-37/386502181/x01/AIP-PT/JAP_ArticleDL_092017/scilight717-1640x440.gif/434f71374e315a556e614141417* jul 2000.

[28] Marisa Di Sabatino, Gaute Stokkan, Birger Retterstø Olaisen, Rune Søndenå, and Øystein Dahl. Characterisation Techniques for Silicon Solar Cells, 2011.

[29] B M Keyes, L M Gedvilas, R Bhattacharya, Y Xu, X Li, and Q Wang. The FTIR Laboratory in Support of the PV Program. (January), 2005.

[30] American Society for Testing and Materials. Standard Practice for Conversion Between Resistivity and Dopant Density for Boron-Doped, Phosphorous-Doped, and Arsenic-Doped Silicon. *Annual Book of ASTM Standards*, F 723-99:1–7, 1999.

[31] Yacine Boulfrad, Antti Haarahiltunen, Hele Savin, Eivind J. Øvrelid, and Lars Arnberg. Enhanced performance in the deteriorated area of multicrystalline silicon wafers by internal gettering. *Progress in Photovoltaics: Research and Applications*, 23(1):30–36, jan 2015.